

Planarian cell number depends on *Blitzschnell*, a novel gene family that balances cell proliferation and cell death

Eudald Pascual-Carreras^{(1) (2)}, Marta Marin-Barba⁽³⁾, Carlos Herrera-Úbeda^{(1) (2)}, Daniel Font-Martín^{(1) (2)}, Kay Eckelt^{(1) (2)}, Nidia de Sousa^{(1) (2)}, Jordi García-Fernández^{(1) (2)}, Emili Saló^{(1) (2)} & Teresa Adell^{(1) (2)*}

⁽¹⁾ Department of Genetics, Microbiology and Statistics and Institute of Biomedicine, Universitat de Barcelona, Barcelona, Catalunya, Spain.

⁽²⁾ Institut de Biomedicina de la Universitat de Barcelona (IBUB), Universitat de Barcelona, Barcelona, Catalunya, Spain.

⁽³⁾ School of Biological Sciences, University of East Anglia, Norwich Research Park, Norwich, Norfolk, UK.

*Corresponding author: Teresa Adell (tadellc@ub.edu)

Keywords: body size, cell number, growth, regeneration, overgrowth, mTOR

Summary statement

Blitzschnell is a novel gene family that controls cell number during planarian regeneration and nutrient-dependent growth/degrowth. Its expression depends on food ingestion and mTOR signalling.

Abstract

Control of cell number is crucial to define body size during animal development and to restrict tumoral transformation. The cell number is determined by the balance between cell proliferation and cell death. Although many genes are known to regulate those processes, the molecular mechanisms underlying the relationship between cell number and body size remain poorly understood. This relationship can be better understood by studying planarians, flatworms that continuously change their body size according to nutrient availability. We identified a novel gene family, *blitzschnell* (*bls*), which consists of *de novo* and taxonomically restricted genes that control cell proliferation:cell death ratio. Their silencing promotes faster regeneration and increases cell number during homeostasis. Importantly, this increase in cell number only leads to an increase in body size in a nutrient-rich environment; in starved planarians silencing results in a decrease in cell size and cell accumulation that ultimately produces overgrowths. *bls* expression is down-regulated after feeding and related with the Insulin/Akt/mTOR network activity, suggesting that the *bls* family evolved in planarians as an additional mechanism by which to restrict cell number in nutrient-fluctuating environments.

Introduction

During embryonic development all species undergo dramatic increases in size until reaching a definitive body size, which is strikingly similar across species. The definitive body size of an organism is reached by increasing either cell number or cell size. Changes in cell size have been described in specific organs, e.g. imaginal discs in *Drosophila* (Miyaoaka *et al.*, 2012; Hariharan, 2015). However, regulation of cell number, achieved by modulating the balance between cell death and cell proliferation, is the main mechanism by which animals reach their definitive body size (Guertin and Sabatini, 2006). Although conceptually simple, the developmental mechanisms that control cell number constitute one of the more intriguing questions in biology. In general, the main signalling pathways thought to control growth regulate cell proliferation and cell death in response to the nutritional environment. Studies in multiple species have identified the same key signalling pathways that appear to regulate body size: the JNK pathway, the Hippo pathway, and the insulin/Akt/mTOR signalling network. The JNK signalling pathway controls cell death and proliferation, mainly in response to cellular stress (Dhanasekaran and Reddy, 2017). The Hippo signalling pathway regulates proliferation, apoptosis, and cell differentiation in response to mechanical stimuli (Udan *et al.*, 2003; Zeng and Hong, 2008). Genetic perturbation of JNK or Hippo signalling leads to overgrowths or organ size changes but does not affect overall body size (Tumaneng *et al.*, 2012; Willsey *et al.*, 2016). In contrast, activation of the insulin/Akt/mTOR signalling network leads to increases in body size in animals as distant as *Drosophila* and mice (Saxton and Sabatini, 2017). The insulin/Akt/mTOR signalling is the most conserved molecular mechanism that relates nutrient intake and cell proliferation (Gokhale and Shingleton, 2015), and it is the main regulator of cell size in response to cellular amino acid levels (González and Hall, 2017; Wolfson and Sabatini, 2017).

The study of planarians, flatworms that display amazing cell plasticity, can help further our understanding of the molecular mechanisms that control body size during development. In most animals adult body size is determined by growth during embryonic and juvenile stages, while the adult stage consists of tissue renewal. However, long-living species such as planarians change their body size according to nutrient availability during their entire lives. These alterations in planarian body size are mediated by changes in cell number (Bagunyà and Romero, 1981; Thommen *et al.*, 2019) resulting from modulation of the balance between cell proliferation and apoptosis. Thus, the ratio of proliferation to apoptosis decreases in starvation conditions and increases in times of nutritional abundance (Baguña, 1976; Pellettieri *et al.*, 2010). Planarian plasticity is sustained by a population of pluripotent adult stem cells (neoblasts) that can differentiate into any planarian cell type. Furthermore, the balance between the stem cell population and all types of differentiated cells relies

on robust signalling mechanisms that allow continuous adjustment of cell proliferation, cell death, and cell differentiation. The signalling pathways that determine cell fate and tissue patterning in planarians, including the Wnt and BMP pathways, have been extensively studied (Molina *et al.*, 2011; Sureda-Gómez, Martín-Durán and Adell, 2016). However, the mechanisms that control planarian body size and growth remain to be fully elucidated. The insulin/mTOR pathway is the only pathway demonstrated to control planarian body size. Inhibition of insulin-like peptides or TOR attenuates cell proliferation, prevents planarian growth after feeding, and accelerates shrinking during starvation (Miller and Newmark, 2012; Tu, Pearson and Sánchez Alvarado, 2012). Hyper-activation of mTOR using *PTEN* or *smg-1* RNA interference (RNAi) does not give rise to larger organisms but does promote over-proliferation and outgrowth formation (Oviedo *et al.*, 2008; González-Estévez, D. A. Felix, *et al.*, 2012). In planarians, *JNK* is required for organ remodelling through the induction of apoptotic cell death (Almuedo-Castillo *et al.*, 2014). Moreover, *hippo* inhibition increases mitosis, inhibits apoptosis, and promotes dedifferentiation, leading to the formation of overgrowths but not to changes in body size or cell number (de Sousa *et al.*, 2018). Planarian plasticity not only facilitates adaptation to the environment but also enables reproduction: most species reproduce asexually through fissioning the tail, producing 2 segments from which two complete organisms regenerate. Amputation in planarians triggers tightly controlled apoptotic and mitotic responses (Baguña and Salo, 1984; Pellettieri *et al.*, 2010; Wenemoser and Reddien, 2010). Silencing of several signalling pathways, such as the JNK or TOR pathways, results in the formation of smaller blastemas in which cell proliferation, apoptosis, and/or differentiation is impaired (Peiris *et al.*, 2012; Tu, Pearson and Sánchez Alvarado, 2012; Almuedo-Castillo *et al.*, 2014). Interestingly, TOR hyper-activation gives rise to larger blastemas, although they remain undifferentiated (González-Estévez, D. A. Felix, *et al.*, 2012), and Hippo hyper-activation enhances the wound response, promoting the expansion of cell populations (Lin and Pearson, 2017).

Here, we describe the identification of a novel gene family that we have named *blitzschnell* (*bls*), which controls cell proliferation and cell death in intact and regenerating planarians. The *bls* family consists of 11 genes and 4 pseudogenes that can be classified into 5 subfamilies (*bls1-5*). The family is composed of *de novo* genes, which appear to be taxonomically restricted to the order Tricladida (commonly known as planarians). Silencing of *bls2/3/5* promotes faster regeneration and increases cell number during homeostasis. However, this increase in cell number leads to an increase in body size only in nutrient-rich environments: during starvation cells are unable to maintain their normal size and become smaller than those of control animals. Importantly, expression of *bls2*, *bls3*, and *bls5* is down-regulated after nutrient intake, and it was found to be related with the Insulin/Akt/mTOR

network, suggesting that in planarians the *bls* family may have evolved as an additional mechanism to restrict cell number in nutrient-fluctuating environments.

Results

Blitzschnell* is a new gene family organized in 2 clusters of tandem repeats in *Schmidtea mediterranea

We performed an RNAi screen to find candidate genes involved in planarian eye regeneration, and identified an unknown gene whose inhibition resulted in faster regeneration of the eyes after head amputation. We named this gene *Blitzschnell* (*bls*), which means “quick as a flash” in German. Surprisingly, upon attempting to identify the genomic locus of this gene in *Schmidtea mediterranea*, we found that *bls* belongs to a gene family composed of 15 members distributed on 2 distinct genomic scaffolds (Fig. 1A, Table S1).

Although all *bls* sequences shared more than 70% identity (Table S2), a phylogenetic analysis using the nucleotide sequence allowed us to classify *bls* genes into 5 subfamilies (Fig. S1A). Four of these subfamilies (*bls1*, *bls2*, *bls4* and *bls5*) contained 2 putative genes each (named a and b) apparently derived from duplications. Subfamily *bls3* contained 7 *bls* sequences (named *bls3a-g*). These were also apparently derived from recent successive tandem duplications, as suggested by their genomic organization (Fig. 1A) and near identical DNA sequences (Table S1; Table S2). One band of the expected size was successfully amplified using primers spanning the junction between *bls3a* and *bls3b*, confirming the existence of at least 2 repeats (Fig. 1A, Fig. S1B, Table S3). Interestingly, in the repeated block harbouring *bls3* members and in the vicinity of other *bls* genes we identified complete or fragmentary transposon-related genes, including the genes encoding for Reverse transcriptase, RNAse H, and Integrase (Fig. 1A).

By mapping reads from the transcriptome of intact planarians (de Sousa *et al.*, 2018) against the genome of *S. mediterranea* (Grohme *et al.*, 2018), we detected transcripts for subfamilies *bls2*, *bls3*, and *bls5*, but not for subfamilies *bls1* or *bls4* (Fig. S1C). Furthermore, the predicted open reading frame (ORF) for *bls2*, *bls3*, and *bls5* encoded peptides containing an N-terminal signal peptide (SP), suggesting that they could be secreted, and a highly conserved C-terminal coiled-coil (CC) domain (Fig. 1B, Table S4). Non-detectable transcription, together with a much shorter ORF, strongly suggests that subfamilies *bls1* and *bls4* are made up of pseudogenes (Ψ).

Taken together these data demonstrate that *bls* is a new gene family consisting of 11 genes and 4 pseudogenes. The genes encode very similar peptides that may be released into the extracellular space, as suggested by the presence of a signal peptide.

The *bls* family is taxonomically restricted to Tricladida

A BLAST search using *S. mediterranea bls* sequences against non-redundant transcriptomic and proteomic databases of all species (NCBI) produced no significant results. More specific BLAST searches against genomic and transcriptomic datasets for Platyhelminth species (Egger *et al.*, 2015) (NCBI and Planmine) indicated that homologs of the *bls* family are only found in species of the order Tricladida (planarians) (Fig. S1D; Table S5): *Schmidtea polychroa* (*Spol*), *Dugesia japonica* (*Djap*), and the sexual *S. mediterranea* strain (*Smes*). Although genomic databases are only available for a few Lophotrochozoa species, this result suggests that the *bls* family is taxonomically restricted to order Tricladida. Interestingly, a BLAST search of the available transcriptomic databases for Tricladida species returned more than one hit for those species (Fig. 1C), with a high degree of similarity at the nucleotide level (Table S6). Phylogenetic analysis performed with amino acid sequences (Table S7) revealed that the *bls5* subfamily was present in all Tricladida species studied, the *bls3* subfamily was present in *Smed*, *Spol*, and *Djap*, and the *bls2* subfamily was present only in *Smed* (Fig. 1C, Fig. S1E). However, it should be borne in mind that transcriptomic databases for Tricladida species other than *Smed* are incomplete.

These findings suggest that the *bls* family is taxonomically restricted to Tricladida.

Subfamilies *bls2*, *bls3*, and *bls5* are expressed in secretory cells

Although the 3 transcribed *bls* subfamilies (*bls2*, *bls3*, and *bls5*) shared a high percentage of sequence identity at nucleotide level (Table S2), we designed riboprobes spanning different gene regions (Table S3; Table S8) to specifically detect genes from each subfamily. Whole-mount *in situ* hybridization (WISH) with each riboprobe revealed the same pattern of expression and labelled specific dorsal-prepharyngeal cells (Fig. 2A, Fig. S2A). Double fluorescence *in situ* hybridization (FISH) revealed coexpression of genes from the 3 families in the same cells although showing not identical subcellular localization (Fig. S2B), confirming riboprobe specificity.

The *bls3* riboprobe revealed that *bls+* cells were located dorsally and in the marginal cells throughout the body (Fig. 2A). These *bls+* cells were differentiated, since they were insensitive to irradiation (Fig. S2C), and corresponded to secretory cells, since they co-expressed *dd4277*, a secretory and parenchymal cell marker (Fincher *et al.*, 2018; Plass *et al.*, 2018) (Fig. 2B). *bls3* was not expressed in blastemas during regeneration, but re-established its expression pattern according to the remodelling of the fragment in question (Fig. S2D). Interestingly, WISH in sexual *S. mediterranea* (*Smes*) and *S. polychroa* (*Spol*) revealed the same expression pattern as observed for *Smed* (Fig. S2E), supporting a conserved function among Tricladida species (Fig. 1C).

Taken together, our data indicate that genes from subfamilies *bls2*, *bls3*, and *bls5* are expressed in a specific subpopulation of secretory prepharyngeal cells in planarians.

***bls* inhibition promotes faster regeneration**

Because *bls2*, *bls3*, and *bls5* genes share a high percentage of identity (Table S2), specific inhibition of any of these genes using RNAi was technically impossible. Furthermore, the high level of shared identity and cellular colocalization (Fig. S2B) suggested that at least some paralogs may perform similar functions. For this reason we designed double-stranded RNAs (dsRNAs) corresponding to a highly conserved region in order to inhibit genes of each of the 3 subfamilies (Fig. S3B; Table S8). qPCR analysis using primers specific to each subfamily (Fig. S3B) showed that expression levels of each of the 3 subfamilies were down-regulated after RNAi (Fig. S3A, S3C). Sequencing of the fragments amplified by each qPCR corroborated inhibition of the genes of each of the 3 subfamilies (see Materials and Methods; Fig. S3C). These animals are referred to henceforth as *bls2/3/5*(RNAi) animals.

RNAi of *bls2/3/5* confirmed our initial observation of faster regeneration after head amputation in planarians. We observed earlier differentiation of the eye spots (Fig. S3D), and earlier differentiation of photoreceptor cells (identified by anti-arrestin immunostaining): after 3 days of regeneration (3dR) the optic chiasm was visible in most *bls2/3/5*(RNAi) animals but not in control animals (Fig. 3). In addition to the visual system, other anterior structures such as the brain branches and chemoreceptors regenerated faster than controls (Fig. 3), as evidenced by quantification of *gpas+* (Cebrià *et al.*, 2002) and *cintillo+* (Oviedo, Newmark and Sánchez Alvarado, 2003) cells, respectively. Quantification of *pitx+* cells (Currie and Pearson, 2013; März, Seebeck and Bartscherer, 2013) revealed an increase the number of differentiated neural cells in the blastema of *bls2/3/5*(RNAi) planarians as early as 18 hours of regeneration (hR) (Fig. S3E). These results demonstrate that inhibition of *Smed-bl2/3/5* promotes faster regeneration.

***bls* attenuates cell proliferation and promotes cell death after injury**

To understand the mechanism by which *Smed-bl2/3/5*(RNAi) promotes faster regeneration, we analysed the proliferative and apoptotic responses triggered by amputation. In planarians, amputation triggers a general proliferative response, which peaks at 6 hR, and a local response that peaks at 48 hR. Quantification of mitotic cells using an anti-phospho-histone 3 (PH3) antibody (Wenemoser and Reddien, 2010) revealed an increase in the mitotic response at both 6 hR and 48 hR in *bls2/3/5*(RNAi) versus control animals (Fig. 4A). The apoptotic response after amputation consists of 2 apoptotic peaks: one at 4 hR, which occurs close to the wound, and a second at 3 days of regeneration (dR), which is generalized (Pellettieri *et al.*, 2010). Using a TUNEL assay (Fig. 4B) and by

quantifying caspase-3 enzymatic activity (Fig. 4C) we demonstrated lower rates of apoptosis in *bls2/3/5*(RNAi) versus control planarians at both time points.

Distinct molecular and cellular responses are induced during healing of amputated tissue, notches (which imply tissue loss), and incisions (in which no tissue is removed). While control of cell proliferation and cell death is required in all scenarios, incision gives rise to just the first proliferative and apoptotic peaks. To examine how general was the role of *bls2/3/5* in attenuating cell proliferation and promoting cell death, we analysed the response to notching and incision in *bls2/3/5*(RNAi) animals. In both situations, compared with controls RNAi animals showed an increase in the number of mitotic cells (Fig. S4A, S4C) and a decrease in apoptosis (Fig. S4B, S4D), indicating that *bls2/3/5* attenuates proliferation and promotes cell death.

These findings indicate that *Smed-blis2/3/5* attenuates cell proliferation and promotes cell death after any injury type, regardless of whether tissue is removed.

Cells are more numerous but smaller in starved *bls*(RNAi) planarians, resulting in no overall change in body size

The pattern of *bls2*, *bls3*, and *bls5* expression in secretory cells in the prepharyngeal region and along the planarian margin suggests that these peptides may play a role in controlling cell proliferation and cell death, not only after injury but also during homeostasis, since planarians undergo continuous growth and degrowth according to nutrient availability. These changes in size are thought to be primarily due to modulation of cell number (Bagunyà and Romero, 1981; Thommen *et al.*, 2019) through regulation of the balance between proliferation and apoptosis (Pellettieri *et al.*, 2010; González-Estévez, D. a. Felix, *et al.*, 2012). In nutrient-poor environments planarians shrink by decreasing mitosis and increasing cell death. To determine whether *bls2/3/5* participates in regulating the proliferation/apoptosis equilibrium and body size during degrowth, we injected starved animals with *bls2/3/5* dsRNA for 3 weeks (Fig. 5A, S5A). The number of PH3+ nuclei found in starved *bls2/3/5* RNAi animals versus control was only increased after the third week (Fig. 5B, S5C). Importantly, starved *bls2/3/5*(RNAi) planarians showed decreased apoptosis since the first week of inhibition compared with controls (Fig. 5C, S5D).

While this alteration in the proliferation/apoptosis equilibrium did not give rise to larger animals (Fig. 5D), total cell number was higher in RNAi-injected animals versus controls (Fig. 5E). The fact that total cell number but not body size was increased in *bls2/3/5*(RNAi) animals implies a decrease in cell size. To examine changes in cell size we focused our analysis on the epidermis, since epidermal cells form a monolayer that can be easily imaged in 3 dimensions. Nuclear staining revealed a higher density of

epithelial cells in *bls2/3/5*(RNAi) animals (Fig. 5F, S5E), and quantification of mean epidermal cell area confirmed that this parameter was reduced in *bls2/3/5*(RNAi) animals as compared with controls (Fig. 5F'). A decrease in mean epidermal cell area could be due not to a reduction in the total cell volume but to narrowing of the cells in *bls2/3/5*(RNAi) animals. To quantify epidermal cell volume we measured epidermal cell height (i.e., the mean distance from the apical to the basal margin of the cell) in animals immunostained with 6G10 antibody. We observed no differences in apical-basal distance in *bls2/3/5*(RNAi) animals with respect to controls (Fig. 5G, 5G'). Multiplication of mean cell area by mean cell height confirmed a decrease in epidermal cell volume in *bls2/3/5*(RNAi) animals versus controls (Fig. 5H, 5I). Changes in specific neural populations were evaluated by confocal imaging (Fig. 5J, S5F) and qPCR (Fig. S5G). The density of serotonergic (*pitx+*) (Currie and Pearson, 2013; März, Seebeck and Bartscherer, 2013), octapaminergic (*tbh+*) (Eisenhoffer, Kang and Alvarado, 2008), dopaminergic (*th+*) (Fraguas, Barberán and Cebrià, 2011) neurons and of chemoreceptors (*cintillo+*) (Oviedo, Newmark and Sánchez Alvarado, 2003) was increased in *bls2/3/5*(RNAi) animals. Given the increase in cell density found in *bls2/3/5*(RNAi) animals after 3 weeks of inhibition, it could be that the increase in PH3+ cells found at this time point results from the cell accumulation rather than from an effect of *bls2/3/5*(RNAi) on mitotic activity. This hypothesis is supported by the finding that the number of PH3+ cells/area normalized by epidermal cell density of *bls2/3/5*(RNAi) is not significantly different from controls after 2 and 3 weeks of inhibition (Fig. S5H).

Importantly, continuous inhibition of *bls2/3/5*(RNAi) for 4 weeks resulted in the formation of overgrowths that were all located in the posterior part of the animal, mainly in the dorso-ventral margin (Fig. 5K). The molecular analysis of those overgrowths demonstrates the accumulation of postmitotic cells (PIWI+, *h2b-*) (Solana *et al.*, 2012), which express epidermal progenitor cell markers (*nb21+*, *agat1+*) (Eisenhoffer, Kang and Alvarado, 2008)(Fig. 5K, SF 5I).

These data indicate that *bls2/3/5* promotes cell death during periods of shrinkage. *bls2/3/5* inhibition in starved planarians prevents the necessary reduction in cell number. Because cell size is reduced in *bls2/3/5*(RNAi) versus control animals, the increase in cell number observed in the former does not translate to larger body size. However, the accumulation of cells following long term inhibition does lead to overgrowths.

***bls* RNAi in fed planarians results in increases in cell number and body size**

Planarians grow in size in nutrient-rich environments. This growth is due to an increase in cell number resulting from an increase in the mitosis:apoptosis ratio (Pellettieri *et al.*, 2010; González-Estévez, D. a. Felix, *et al.*, 2012). Our previous findings suggest that *bls2/3/5* inhibition in continuously fed planarians may lead to an increase in cell number and possibly also in body size. To test this hypothesis, planarians fed twice per week were injected with *bls2/3/5* dsRNA for 3 weeks (Fig. 6A, S6A, S6B). Compared with controls, these animals showed an increase in the rate of mitosis from the first week of inhibition (Fig. S6C, 6B, S6C), together with a decrease in the rate of apoptosis (Fig. 6C, S6E). Furthermore, during this 3-week period RNAi animals grew faster and reached a larger size (Fig. 6D) than controls (Fig. 6E). Quantification of dissociated cells revealed an increase in total cell number in *bls2/3/5*(RNAi) animals after 3 weeks of RNAi (Fig. 6F). In contrast to the results obtained for starved planarians, no differences in epidermal cell area or volume were observed in fed animals with respect to controls (Fig. 6G-J, S6F). Furthermore, quantification of neural and chemoreceptor cells revealed no differences in cell density between RNAi and control planarians (Fig. 6K, S6G).

These data indicate that *Smed-bls2/3/5* also promotes cell death and attenuates the rate of mitosis during growth periods, resulting in an increase in cell number. Remarkably, in fed animals this increase in cell number translates to an increase of body size, since cell size is maintained in this nutrient rich context.

***bls* transcription depends on nutrient intake and mTOR signalling**

Our results demonstrate that *bls2/3/5* subfamilies control the balance of cell proliferation and cell death in planarians not only after injury but also during normal homeostasis. We hypothesize that *bls2/3/5*-mediated signalling may constitute a general mechanism required to balance cell proliferation:cell death ratio in response to nutrient availability in planarians. According to our hypothesis, *bls2/3/5* activity would be required in nutrient-poor environments but not when food is readily available. As previously mentioned, planarian growth is sustained by increasing mitosis and decreasing cell death. After feeding, apoptosis remains very low and changes little (Fig. S7A), but proliferation increases and mitosis peaks at 3 hours post-feeding (hpf) (Baguñà, 1974; Newmark and Sánchez Alvarado, 2000) (Fig. S7B). Thus, according to our hypothesis, *bls* expression should be actively down-regulated a few hours after food ingestion to enable subsequent growth. Quantification of mRNA levels of *bls2*, *bls3*, and *bls5* by qPCR at 3 hpf and 24 hpf revealed down-regulation of all 3 *bls* mRNAs (Fig. 7A). This down-regulation was also confirmed by FISH expression analysis: after

feeding (24 hpf) expression of all 3 genes had decreased and/or the expression pattern had expanded and delocalized with respect to starved conditions (Fig. 7B, S7C, S7D).

To further understand the mechanism by which *bls2/3/5* balances cell proliferation:cell death ratio in response to nutrient intake, we analyzed its possible functional interaction with the mTOR pathway, a central regulator of cell metabolism (Saxton and Sabatini, 2017). In planarians mTOR is up-regulated in response to food intake, and its inhibition decreases proliferation and increases cell death, impeding growth (Peiris *et al.*, 2012; Tu, Pearson and Sánchez Alvarado, 2012). Quantification of *bls2*, *bls3*, and *bls5* expression levels in growing mTOR (RNAi) planarians shows a significant increase of *bls2*, *bls3*, and *bls5* mRNA expression levels (Fig. 7C). Furthermore, quantification of mTOR expression levels in growing *bls2/3/5* (RNAi) animals shows up-regulation of mTOR mRNA levels (Fig. 7D). Akt is a serine threonine protein kinase downstream of Insulin and upstream of mTOR pathway (Yoon, 2017), which inhibition in planarians increases cell death, decreases proliferation and impedes planarian growth (Peiris *et al.*, 2016). qPCR quantification of *Akt* levels also demonstrates its up-regulation in *bls2/3/5* RNAi planarians (Fig.7D).

Overall, these suggest that expression of *bls2/3/5* subfamilies are constantly regulated in planarians to balance the cell proliferation:cell death ratio, being down-regulated by nutrient intake to allow planarian growth. *bls2/3/5* is a novel gene that regulates cell number in response to nutrient intake, but it interacts with the evolutionary conserved Insulin/Akt/mTOR metabolic network.

Discussion

***bls* is a *de novo* gene family taxonomically restricted to the order Tricladida (planarians)**

In this study we have identified a new gene family, *blitzschnell* (*bls*), which appears to be an evolutionary novelty of Triclad (planarians), and is essential for the control of cell number in response to nutrient intake. In *S. mediterranea*, *bls* family is composed by 15 members, grouped in 5 subfamilies (*bls1-5*). Members of *bls1* and *bls4* subfamilies are pseudogenes, while members of *bls2*, *bls3* and *bls5* subfamilies encode for short peptides that contain a signal peptide (SP) and a coiled coil domain (CC). FISH analysis with specific riboprobes, demonstrates that *bls2*, 3 and 5 are all expressed in a subset of secretory cells, seeming tissue specific. Furthermore, we have only been able to find homologs of *bls* in species of the Tricladida order. Although the genomic databases of Platyhelminthes are incomplete, *bls* family appears to be Taxonomically restricted (Wilson *et al.*, 2005). All described features: gene duplication and presence of pseudogenes (Tautz and Domazet-Lošo, 2011), short open reading frame

with a signal peptide and a ISD (Neme and Tautz, 2013; Palmieri, Kosiol and Schlötterer, 2014; Wilson *et al.*, 2017; Werner *et al.*, 2018), being expressed in specific cell types (Toll-Riera *et al.*, 2009; Carvunis *et al.*, 2012; Zhao *et al.*, 2014), and being Taxonomically restricted (Van Oss and Carvunis, 2019), are shared by genes that originated *de novo* during evolution. *de novo* genes, previously known as orphan genes (Schlötterer, 2015), could originate from an existing gene in the genome (Long *et al.*, 2003), from non codifying genomic regions (Schlötterer, 2015), or from transposon domestication (McLysaght and Hurst, 2016). Although further phylogenetic studies are required to understand the origin of *bls* family, our data favours the last two possibilities, since we could not find any homolog in species outside Tricladida, and we found transposable elements in the same genomic region where *bls* family is found.

The appearance of *bls* in Tricladida may be linked to the requirement for continuous and rapid modulation of cell number in response to nutrient availability.

Our results demonstrate that *bls2/3/5* regulates the mitosis:apoptosis ratio in all scenarios analysed. In homeostatic animals, the imbalance in this ratio led to an increase in cell number. Strikingly, this increase in cell number resulted in normal body size but smaller cell size in starved planarians, and in larger body size and normal cell size in fed animals (Fig. 8), suggesting an energy-dependent role of this gene. In other organisms *de novo* genes have been shown to play an important role in the response to biotic and/or abiotic stresses (Colbourne *et al.*, 2011; Donoghue *et al.*, 2011; Zhao *et al.*, 2014). The observation that *bls2*, *bls3*, and *bls5* are down-regulated few hours after food ingestion suggests that those genes can function as sensors of cell energy status. According to this hypothesis, *bls* expression is required to restrict cell number (and maintain cell size) in starvation conditions, but is down-regulated after nutrient intake to allow for increases in cell number and body size (Fig. 8). The appearance of *bls* in Tricladida during evolution may be linked to the requirement for continuous modulation of cell number in response to nutrient availability in these organisms. The increase in the number of copies of *bls* family members and their tandem disposition suggest that they may be regulated by the same promoter, facilitating rapid regulation of their protein levels according to cell energy status.

Because *bls* genes share 70–100% of identity at the nucleotide level, we were unable to inhibit specific copies using RNAi, and were therefore unable to determine which gene copies perform the described function. For this reason, in this study we have ascribed this function to “*bls2/3/5*”. However, because all *bls* genes appear to follow the same expression dynamics and share almost identical amino acid sequences, we hypothesize that the gene copies encoding the SP and CC domains may perform the

same function. This is in agreement with the aforementioned hypothesis of simultaneous regulation enabling rapid changes in expression. Nonetheless, we cannot rule out the possibility that copies that do not encode the CC domain may act as inhibitors.

***bls* could control the mitosis:apoptosis ratio and the cell size through interacting with the insulin/Akt/mTOR network.**

It has been described that *de novo* and TRG lack catalytic domains and normally interact with proteins in conserved networks (Arendsee, Li and Wurtele, 2014). The presence of a SP suggests that *bls2*, *bls3*, and *bls5* may be secreted and interact with components of those conserved pathways. Our results suggest that *bls2/3/5* may interact with members of the insulin/Akt/mTOR pathways, a universal mechanism that is activated by the extracellular nutrients and activates the signals required for growth. In planarians TORC-1 is down-regulated during starvation and its inhibition decreases proliferation without affecting cell death. mTOR is up-regulated in response to food intake in planarians, and its inhibition decreases proliferation and increases cell death, impeding growth (Peiris *et al.*, 2012; Tu, Pearson and Sánchez Alvarado, 2012). mTOR hyper-activation, through PTEN or *smg-1* RNAi, promotes over-proliferation and outgrowths (Oviedo, Newmark and Sánchez Alvarado, 2003; González-Estévez, D. a. Felix, *et al.*, 2012). Since *bls2/3/5* is expressed in nutrient-deprived conditions, it could be acting as an inhibitor of the insulin/Akt/mTOR network, which is in fact what our results suggest; mTOR and Akt are up-regulated when *bls2/3/5* is inhibited, and vice versa.

An important result in this study is the finding that cellular responses are different according to the energetic status of the animals. *bls2/3/5* inhibition during starvation results in an early decrease in apoptosis and, with our methods, we could not detect an increase in mitotic index. In contrast, in growing animals both parameters seem to be affected. This could be also true when modulating the mTOR pathway, and the reason why different studies show opposite results regarding the mitotic rates mTOR silencing during homeostasis (Peiris *et al.*, 2012; Tu, Pearson and Sánchez Alvarado, 2012). Cell death and proliferation analysis from specific nutritional context are required to understand the metabolic role of those signals.

Similarly, only in fed animals cells are able to maintain the size after *bls2/3/5* inhibition. One possible explanation for the inability of starved animals to maintain cell size is that *bls2/3/5* silencing in these conditions may promote entry into M phase before cells reach their proper size. It is possible that in wild-type planarians cell cycle length varies according to nutritional status. Recent data suggest the existence of crosstalk between cell division and mitochondrial dynamics and metabolic pathways (Salazar-Roa and Malumbres, 2017). For example, yeast grown in nutrient-poor conditions adjust their

cell-cycle duration to accommodate slower growth, so that the size at which cells divide is similar to that observed in nutrient-rich environments (Lloyd, 2013). It is possible that the duration of the cell cycle is longer in starved than fed animals, thereby ensuring that daughter cells reach the appropriate size. Promoting entry into M phase after *bIs2/3/5* silencing could give rise to smaller cells in starved but not in fed animals. Since a mechanism through which mTOR signals regulate cell size is by controlling cell cycle (Fingar *et al.*, 2002), and as described above planarian mTOR activity is regulated by food intake, interaction of *bIs2/3/5* with this pathway could account for the smaller size of cells in starved animals. Analysis of the cell cycle in each of these different conditions will be required to test this hypothesis.

***bIs* is a tumour suppressor, inhibition of which favours regeneration**

The appearance of overgrowths in starved *bIs2/3/5* RNAi animals could be a consequence of the increase in cell density promoted after sustained inhibition cell death, as observed in tumoral processes (Lowe and Lin, 2000). *bIs* thus acts as a tumour suppressor during planarian degrowth. This observation presents us with a paradox: although caloric restriction extends lifespan (Pifferi and Aujard, 2019), in *bIs2/3/5*(RNAi) planarians food deprivation promotes hyperplasia and the formation of overgrowths, while fed *bIs2/3/5*(RNAi) animals only increase body size with no apparent changes in patterning. A second key observation is that while *bIs2/3/5* inhibition in starved animals promotes overgrowths, it favours regeneration after any kind of injury. This is consistent with the view that tumour suppressors evolved not to suppress tumour growth but to control cellular processes such as proliferation, cell death, and cell differentiation, which are essential during embryogenesis and are activated during regeneration of complex tissues (Nacu and Tanaka, 2011). Perturbation of tumour suppressor function can enhance the regeneration of somatic stem cells in the hematopoietic system or endocrine cells (Pomerantz and Blau, 2013). Furthermore, inhibition of the Hippo pathway and consequent YAP/TAZ activation results in increases in organ size and promotes tumour formation in adult mice, but also promotes regeneration of the liver, gut, muscle, and heart in mouse models (Moya and Halder, 2019).

Silencing of several known vertebrate tumour suppressors including mTOR, p53, and Hippo, also induces the formation of overgrowths in planarians, but despite increasing proliferation does not promote proper regeneration. While TOR hyper-activation results in larger blastemas, these remain undifferentiated (González-Estévez, D. a. Felix, *et al.*, 2012). Hippo hyper-activation also enhances the wound response and promotes expansion of the epidermal and muscle cell populations and regeneration of larger structures such as the eyes (Lin and Pearson, 2017). However, this new tissue

is not properly patterned (de Sousa *et al.*, 2018). *bIs* is the first gene described whose inhibition promotes faster but apparently normal regeneration. One possible explanation is that *bIs* specifically controls cell number (through regulation of the cell proliferation:cell death ratio) but not cell differentiation, as described for other signalling pathways such as Hippo (de Sousa *et al.*, 2018). In this scenario, an increase in the number of cells during early stages of regeneration could accelerate the expression of wound-induced genes (Wenemoser *et al.*, 2012), as we observed for *pitx*, and thereby promote more rapid appearance of regenerated structures.

Conclusion

In most animal species the adult stage is distinguished from the embryonic stage by the maintenance of body size, cell number, and proportions. However, long-lived animals such as planarians continuously regulate body size in adulthood by controlling cell number according to nutrient availability. Thus, the mechanisms described for other organisms, such as *Drosophila*, in which tissues “know” their final size, may not apply to planarians (Nowak *et al.*, 2013). Given that nutrient availability always fluctuates in nature, the *bIs* family may represent an example of *de novo* genes that evolved in planarians to fulfil the requirement for continuous regulation of cell number according to nutrient availability. Other *de novo* genes have been implicated in increasing the fitness of the organism (Reinhardt *et al.*, 2013; Schlötterer, 2015). Examples are described in cnidarians, in which *Hym301* regulates tentacle number (Khalturin *et al.*, 2008), and in molluscs, in which each species expresses a unique set of secreted proteins that drives shell diversity (Aguilera *et al.*, 2017). *De novo* genes are usually integrated into existing pathways, adding additional levels of regulation. *bIs* genes may interact with members of the insulin/Akt/mTOR signalling pathways, which regulate growth in response to nutrient intake in planarians and in vertebrates. RNAi of components of these pathways does not fully phenocopy *bIs2/3/5* RNAi. However, this signalling pathway should be thought of as a network in which each of these signals functions in a complex and dynamic manner, as opposed to a linear pathway. Future studies will need to determine whether the primary function of *bIs* is to control proliferation, apoptosis, or both, and to elucidate the molecular integration of *bIs* within the insulin/Akt/mTOR network. Given that the molecular signals controlling body and organ growth are also key players in most human cancers, understanding the mechanism by which *bIs* genes act as tumour suppressors would help identify novel targets for the design of therapeutic strategies to modulate tissue growth.

Materials and methods

Planarian culture

The planarians used in this study are the asexual clonal strain of *S. mediterranea* BCN-10 biotype and were maintained as previously described (Fernandéz-Taboada *et al.*, 2010) in PAM water (Cebrià and Newmark, 2005). Animals were fed twice per week with liver, and those used in starvation experiments were starved for 1 week.

RNAi screening

To identify genes involved in eye regeneration we performed a high density DNA microarray. We ran a gene expression profile of planarian tissues with control animals (control RNAi) and planarians without eyes (*Smed-sine oculis* RNAi) during early stages of head regeneration using the “array star” software from Nymbelgene. 61 candidate genes differentially expressed in those conditions were analyzed by RNAi (Eckelt, 2011). Among them we isolated *Smed-bls3*, which inhibition produced a faster eye regeneration.

Sequence and phylogenetic analyses

A fragment of *Smed-bls3* was identified from (Eckelt, 2011). Other members of the families were identified from the genome (Grohme *et al.*, 2018) and amplified using specific primers (Table S3). The signal peptide was identified with SigalP v5.0 (Almagro Armenteros *et al.*, 2019) and the coiled-coil domain was characterized using the tool available online from PRABI (Pole Rhone-Alpes de Bioinformatique; https://npsa-prabi.ibcp.fr/cgi-bin/npsa_automat.pl?page=npsa_lupas.html) (Lupas, Van Dyke and Stock, 1991). Sequence identity comparison was carried out using the pairwise alignment tool in Jalview suite v2.11 (Waterhouse *et al.*, 2009).

To determine which members of each family were expressed, we mapped the RNAseq paired reads from adult wild-type animals (de Sousa *et al.*, 2018) against assembly 2 of the *S. mediterranea* genome (Grohme *et al.*, 2018) using *Bowtie2* (Langmead *et al.*, 2009) v2.3.4, selecting the *-end-to-end* option. After alignment, we extracted the reads mapping the scaffolds of interest using *samtools view* (Li *et al.*, 2009) v1.9. The final assessment was performed manually using the Integrative Genomics Viewer (Robinson *et al.*, 2011) (IGV v2.4.4) to verify the families with mapped reads.

Sequence comparison against the GenBank database was performed using the NCBI BLAST network server (<http://www.ncbi.nlm.nih.gov/Structure/cdd/wrpsb.cgi>). Potential orthologs were searched for using tBLASTx where possible to allow a certain level of tolerance in case of a high degree of

divergence. The search for orthologs was performed against transcriptomes and genomes from several Platyhelminthes species (Table 4) (Egger *et al.*, 2015).

The IQ-tree web server (Trifinopoulos *et al.*, 2016) was used to reconstruct the phylogenetic relationships between *Smed-bls* families. The nucleotide or protein sequences were first aligned using the alignment servers in JalView suite (MUSCLE for nucleotides and MAFFT for amino acids). Substitution model selection was performed automatically by the software, the number of bootstrap iterations was set to 1500 and default options were selected for the remaining parameters. The trees were visualized using FigTree v1.4.4 (<http://tree.bio.ed.ac.uk/software/figtree/>) with the default parameters.

Whole-mount *in situ* hybridization (WISH)

Probes were synthesised *in vitro* using SP6 or T7 polymerase and DIG- or FITC- modified (Roche). RNA probes were purified by ethanol precipitation and the addition of 7.5 M ammonium acetate. For colorimetric whole-mount *in situ* hybridization (WISH) animals were sacrificed with 5% N-acetyl-L-cysteine (NAC), fixed with 4% formaldehyde (FA), and permeabilized with Reduction Solution. The fixative and WISH protocol used has been previously described (Currie *et al.*, 2016). For whole-mount fluorescent *in situ* hybridization (FISH) animals were sacrificed with 7.5% NAC and fixed with 4% FA. FISH was carried out as described previously (King and Newmark, 2013). For double FISH (dFISH) an azide step (150 mM sodium azide for 45 min at room temperature [RT]) was added. Nuclei were stained with DAPI (1:5000; Sigma). For FISH of paraffin sections animals were sacrificed with 2% HCl and fixed with 4% PFA. Paraffin embedding and sectioning were carried out as previously described (Cardona *et al.*, 2005) and slides were de-waxed, re-hydrated; and antigen retrieval step was performed as previously described (Sureda-Gómez, Martín-Durán and Adell, 2016). Sections were hybridized with the corresponding probes for 16 hours and incubated with antibody diluted 1%BSA, for 16 hours. Both steps were carried out in a humidified chamber (Cardona *et al.*, 2005).

Immunohistochemistry

Whole-mount immunohistochemistry was performed as previously described (Ross *et al.*, 2015). Animals were killed with 2% HCl and fixed with 4% FA. The following antibodies used in these experiments: mouse anti-synapsin (anti-SYNORF1, 1:50; Developmental Studies Hybridoma Bank, Iowa City, IA, USA), mouse anti-VC1 (anti-arrestin, 1:15000, kindly provided by Professor K. Watanabe), rabbit anti-phospho-histone H3 (Ser10) (D2C8) (PH3) (1:500; Cell Signaling Technology) and anti-SMEDWI-1 antibody (1:1000, kindly provided by Professor Kerstin Bartscherer, Hubrecht Institute, Utrecht, Nederland). The secondary antibodies used were Alexa 488-conjugated goat anti-

mouse (1:400; Molecular Probes, Waltham, MA, USA) and Alexa 568-conjugated goat anti-rabbit (1:1000; Molecular Probes). Nuclei were stained with DAPI (1:5000). For immunohistochemistry of paraffin sections animals were killed and treated as described above. Sections were blocked in 1% bovine serum albumin (BSA) in 1X PBS for 1 h at RT and then incubated with primary antibodies diluted in blocking solution (mouse anti-muscle fibre antibody, 6G10, 1:400; Developmental Studies Hybridoma Bank) for 16 h at 4°C in a humidified chamber. Subsequently, sections were washed in 1X PBS and incubated with secondary antibodies (anti-mouse Alexa 488-conjugated antibody, 1:400; Molecular Probes) in blocking solution for 3 h at RT in a humidified chamber. Nuclei were stained with DAPI (1:5000; Sigma).

TUNEL assay

For the whole-mount TUNEL assay animals were sacrificed with 10% NAC, fixed with 4% FA, and permeabilized with 1% sodium dodecyl sulfate (SDS) solution. TUNEL assay was carried out as described previously (Pellettieri *et al.*, 2010) using the ApopTag Red *In situ* Apoptosis Detection Kit (CHEMICON, S7165). Nuclei were stained with DAPI (1:5000; Sigma). For TUNEL assay on paraffin sections animals were killed and treated as described above. Sections were treated as described previously (Pellettieri *et al.*, 2010) and after the dewaxing step a proteinase K step was added for permeabilization. Next, we used the ApopTag Red *In situ* Apoptosis Detection Kit (CHEMICON, S7165). Positive cells were counted in at least 9 representative sagittal sections per animal and the overall mean value was determined. Six animals were analyzed per condition.

RNA interference analysis

Double strand RNA (dsRNA) was synthesised by *in vitro* transcription (Roche) as previously described (Sanchez Alvarado and Newmark, 1999). dsRNA (3 × 32.2 nl) was injected into the digestive system of each animal on 3 consecutive days (1 round). The experiments in which regeneration was studied consisted of 2 consecutive rounds of injections and an amputation at the end of each round. In experiments in which planarians were starved animals underwent 3 or 4 consecutive rounds of injection, without amputation. In experiments involving fed animals, planarians received dsRNA injections on 3 non-consecutive days per week and were fed on the 2 intervening days. This process was repeated for 3 weeks in total. All control animals were injected with dsRNA of green fluorescent protein (GFP). RNAi of subfamilies *bls2*, *bls3*, and *bls5* was carried out using 2 different RNA sequences, both of which produced the same phenotype when injected in regenerating planarians (Table S3; Table S8). The sequences corresponded to the full *bls3* sequence and to a smaller region showing the greatest similarity between the *bls2*, *bls3*, and *bls5* subfamilies. In the case of the second RNA

sequence, inhibition of all members of the transcribed families was demonstrated by qPCR analysis (Fig. S3B-C, S5B, S6B)

Feeding experiments

In long term growth experiments involving RNAi, animals were fed twice per week: food was provided in the morning and removed at the end of the day (Fig. 5A, S5A). PAM water (planarian artificial medium) was replenished three times per week. In RNAi experiments, after 2 weeks of injections in starvation conditions animals were fed for 30 minutes (Fig. 7C). Next, food was removed and PAM water replenished. To study gene expression after feeding we analysed planarians that had been starved for 1 week and then fed for 30 minutes. Next, we removed the food and replenished the PAM water (Fig. 7A). Hours post feeding (hpf) were counted from the moment of removal of the last piece of food.

Quantitative real-time PCR

Total RNA was extracted from a pool of 5 planarians per condition using TRIzol reagent (Invitrogen). cDNA was synthesized as previously described in (Almuedo-Castillo *et al.*, 2014). Expression levels were normalized to that of the housekeeping gene *ura4*. All experiments were performed using 3 biological and 3 technical replicates for each condition. The design of specific primers corresponding to the 5' region for subfamilies *bls2*, *bls3*, and *bls5* allowed verification of the inhibition of the 3 gene families after RNAi. All primers used in this study are shown in Table S3.

Caspase-3 activity assay

For each condition protein extraction was performed in 5 planarians. The protein concentration of the cell lysates was measured using BioRad protein reagent. Fluorometric analysis of caspase-3 activity was performed as described previously (González-Estévez *et al.*, 2007) using 20 mg of protein extract, which was incubated for 2 hours at 37°C with 20 µM caspase-3 substrate Ac-DEVD-AMC or 2 ml from a stock of 1 mg/ml for a final volume of 150 µl. Using a Fluostar Optima microplate fluorescence reader (BMG Labtech) fluorescence was measured in a luminescence spectrophotometer (Perkin- Elmer LS-50), applying the following settings: excitation, 380 nm; emission, 440 nm. Three technical replicates were analysed per condition.

Cell number and cell volume analyses

To quantify total cell number planarian cells were dissociated with trypsin and the nuclei stained with DAPI (Moritz *et al.*, 2012). The cell suspension was transferred to a Neubauer chamber, cells were manually counted 3 occasions, and the mean value calculated. Five planarians were analysed per

biological replicate, and 3 replicates were analysed per condition. Mean cell volume (V) was calculated by multiplying mean epidermal cell area (A) by epidermal cell height (H). To quantify the mean epidermal cell area, the prepharyngeal epidermal area was imaged and the number of nuclei per area was quantified. To determine mean epidermal cell height, the distance between the apical to the basal part of the cell was measured. Measurements were taken in 3 different regions of the same section and the mean value obtained.

Imaging and quantification

Whole-mount WISH, FISH, and immunohistochemistry images were captured with a ProgRes C3 camera from Jenoptik (Jena, TH, Germany). A Leica MZ16F microscope (Leica Microsystems, Mannheim, BW, Germany) was used to observe the samples and obtain FISH, immunostaining, and TUNEL images. A Leica TCS SPE confocal microscope (Leica Microsystems, Mannheim, BW, Germany) was used to obtain confocal images of whole-mount FISH, immunostaining, and TUNEL assays. Representative confocal stacks for each experimental condition are shown. Cell counting of PH3+, TUNEL+ and specific cell types was carried out by eye quantification in a previously defined area of each animal. Areas are schematically indicated in each figure. The total number of positive cells was divided by these areas. Images were blind analyzed and later grouped according to each genotype. To calculate the ratio PH3+cells:epidermal cell density, the number of PH3+ cells/mm² counted per animal was divided by the epidermal cell density quantified in a predetermined prepharyngeal region.

Statistical analyses

Statistical analyses were performed using GraphPad Prism 6. Two-sided Student's t-tests ($\alpha = 0.05$) were performed to compare the means of 2 populations. Two-sided Fisher's exact tests were used to compare 2 phenotypic variants between 2 populations. `fisher.test` from the R package was used to compare more than 2 phenotypic variants between 2 populations.

Statistical data presentation

Results were plotted using GraphPad Prism 6. To compare 2 populations, we used box plots depicting the median, the 25th and 75th percentiles (box), and all included data points (black dots). Whiskers extend to the largest data point within the 1.5 interquartile range of the upper quartile and to the smallest data point within the 1.5 interquartile lower range of the quartile. To plot data points over time we used XY plots, in which each dot represents the mean and bars represent the standard error. Each dot is connected with the next in an arbitrary manner. To visualize the percentage phenotype in each population we used the Stacked Bars plot in R. Each phenotype is assigned a distinct colour.

Acknowledgements

We wish to thank all members of the Emili Saló, Teresa Adell and Francesc Cebrià labs for their suggestions and discussion of the results. We would like to thank PatriK Aloy for tertiary structure prediction of the peptide. Thanks also to Owen Howard for English language editing assistance, and to the anonymous reviewers for their useful comments.

Competing interests

'No competing interests declared'.

Funding

EPC is the recipient of an FPI (Formación del Profesorado Investigador) scholarship from the Spanish Ministerio de Ciencia, Innovación y Universidades. The funder had no role in the study design, data collection and analysis, decision to publish, or manuscript preparation. ES and TA received funding from the Ministerio de Educación y Ciencia (grant number BFU2017-83755-P and BFU2014-56055-P). ES and TA benefits from 2017SGR-1455 from AGAUR (Generalitat de Catalunya). ES received funding from AGAUR (Generalitat de Catalunya: grant number 2009SGR1018). In no case the funder had no role in study design, data collection and analysis, decision to publish, or preparation of the manuscript.

Data availability

GenBank accession numbers of bls sequences are as follows: *bls1a* (BK010973), *bls1b* (BK010974), *bls2a* (BK010975), *bls2b* (BK010976), *bls3a* (BK010977), *bls3b* (BK010978), *bls3c* (BK010979), *bls3d* (BK010980), *bls3e* (BK010981), *bls3f* (BK010982), *bls3g* (BK010983), *bls3e* (BK010984), *bls4a* (BK010985), *bls4b* (BK010986), *bls5a* (BK010987) and *bls5b* (BK010988).

References

- Aguilera, F. *et al.* (2017) 'Co-option and de novo gene evolution underlie molluscan shell diversity', *Molecular Biology and Evolution*, 34(4), pp. 779–792. doi: 10.1093/molbev/msw294.
- Almagro Armenteros, J. J. *et al.* (2019) 'SignalP 5.0 improves signal peptide predictions using deep neural networks', *Nature Biotechnology*. Nature Publishing Group, 37(4), pp. 420–423. doi: 10.1038/s41587-019-0036-z.
- Almuedo-Castillo, M. *et al.* (2014) 'JNK controls the onset of mitosis in planarian stem cells and triggers apoptotic cell death required for regeneration and remodeling.', *PLoS genetics*, 10(6), p. e1004400. doi: 10.1371/journal.pgen.1004400.
- Arendsee, Z. W., Li, L. and Wurtele, E. S. (2014) 'Coming of age: orphan genes in plants', *Trends in Plant Science*. Elsevier Current Trends, 19(11), pp. 698–708. doi: 10.1016/J.TPLANTS.2014.07.003.
- Baguñà, J. (1974) 'Dramatic mitotic response in planarians after feeding, and a hypothesis for the control mechanism', *Journal of Experimental Zoology*, 190(1), pp. 117–122. doi: 10.1002/jez.1401900111.
- Baguñà, J. (1976) 'Mitosis in the intact and regenerating planarian *Dugesia mediterranea* n.sp. I. Mitotic studies during growth, feeding and starvation', *Journal of Experimental Zoology*, 195(1), pp. 53–64. doi: 10.1002/jez.1401950106.
- Baguñà, J. and Saló, E. (1984) 'Regeneration and pattern formation in planarians I. The pattern of mitosis in anterior and posterior regeneration in *Dugesia* (*G*) *tigrina*, and a new proposal for blastema formation', *Development*, 83(1), pp. 63–80. Available at: <https://dev.biologists.org/content/develop/83/1/63.full.pdf> (Accessed: 19 August 2019).
- Bagunyà, J. and Romero, R. (1981) 'Quantitative analysis of cell types during growth, degrowth and regeneration in the planarians *Dugesia mediterranea* and *Dugesia tigrina*', *Hydrobiologia*, 84(1), pp. 181–194. doi: 10.1007/BF00026179.
- Cardona, A. *et al.* (2005) 'An in situ hybridization protocol for planarian embryos: Monitoring myosin heavy chain gene expression', *Development Genes and Evolution*, 215(9), pp. 482–488. doi: 10.1007/s00427-005-0003-1.
- Carvunis, A.-R. *et al.* (2012) 'Proto-genes and de novo gene birth.', *Nature*. NIH Public Access, 487(7407), pp. 370–4. doi: 10.1038/nature11184.
- Cebrià, F. *et al.* (2002) 'Dissecting planarian central nervous system regeneration by the expression of neural-specific genes.', *Development, growth & differentiation*, 44(2), pp. 135–46. Available at: <http://www.ncbi.nlm.nih.gov/pubmed/11940100> (Accessed: 18 June 2018).
- Cebrià, F. and Newmark, P. A. (2005) 'Planarian homologs of netrin and netrin receptor are required for proper regeneration of the central nervous system and the maintenance of nervous system architecture.', *Development (Cambridge, England)*, 132(16), pp. 3691–703. doi: 10.1242/dev.01941.
- Colbourne, J. K. *et al.* (2011) 'The Ecoresponsive Genome of *Daphnia pulex*', *Science*. American Association for the Advancement of Science, 331(6017), pp. 555–561. doi: 10.1126/SCIENCE.1197761.
- Currie, K. W. *et al.* (2016) 'HOX gene complement and expression in the planarian *Schmidtea mediterranea*', *EvoDevo*, 7(1), p. 7. doi: 10.1186/s13227-016-0044-8.
- Currie, K. W. and Pearson, B. J. (2013) 'Transcription factors *lhx1/5-1* and *pitx* are required for the maintenance and regeneration of serotonergic neurons in planarians.', *Development (Cambridge, England)*, 140(17), pp. 3577–88. doi: 10.1242/dev.098590.
- Dhanasekaran, D. N. and Reddy, E. P. (2017) 'JNK-signaling: A multiplexing hub in programmed cell death', *Genes & Cancer*, 8(9). doi: 10.18632/genesandcancer.155.
- Donoghue, M. T. *et al.* (2011) 'Evolutionary origins of Brassicaceae specific genes in *Arabidopsis thaliana*', *BMC Evolutionary Biology*. BioMed Central, 11(1), p. 47. doi: 10.1186/1471-2148-11-47.
- Eckelt, K. (2011) *Multi-approach analysis for identification and functional characterization of eye regeneration related genes of Schmidtea mediterranea*. University of Barcelona, Barcelona, Spain.
- Egger, B. *et al.* (2015) 'A transcriptomic-phylogenomic analysis of the evolutionary relationships of flatworms', *Current Biology*, 25(10), pp. 1347–1353. doi: 10.1016/j.cub.2015.03.034.
- Eisenhoffer, G. T., Kang, H. and Alvarado, A. S. (2008) 'Molecular Analysis of Stem Cells and Their

Descendants during Cell Turnover and Regeneration in the Planarian *Schmidtea mediterranea*', *Cell Stem Cell*, 3(3), pp. 327–339. doi: 10.1016/j.stem.2008.07.002.

Fernández-Taboada, E. *et al.* (2010) 'Smed-SmB, a member of the LSM protein superfamily, is essential for chromatoid body organization and planarian stem cell proliferation.', *Development (Cambridge, England)*, 137(7), pp. 1055–65. doi: 10.1242/dev.042564.

Fingar, D. C. *et al.* (2002) 'Mammalian cell size is controlled by mTOR and its downstream targets S6K1 and 4EBP1/eIF4E', *GENES & DEVELOPMENT*, pp. 1472–1487. doi: 10.1101/gad.995802.when.

Fraguas, S., Barberán, S. and Cebrià, F. (2011) 'EGFR signaling regulates cell proliferation, differentiation and morphogenesis during planarian regeneration and homeostasis.', *Developmental biology*, 354(1), pp. 87–101. doi: 10.1016/j.ydbio.2011.03.023.

Gokhale, R. H. and Shingleton, A. W. (2015) 'Size control: The developmental physiology of body and organ size regulation', *Wiley Interdisciplinary Reviews: Developmental Biology*, 4(4), pp. 335–356. doi: 10.1002/wdev.181.

González-Estévez, C. *et al.* (2007) 'Gtdap-1 promotes autophagy and is required for planarian remodeling during regeneration and starvation.', *Proceedings of the National Academy of Sciences of the United States of America*, 104(33), pp. 13373–8. doi: 10.1073/pnas.0703588104.

González-Estévez, C., Felix, D. a., *et al.* (2012) 'Decreased neoblast progeny and increased cell death during starvation-induced planarian degrowth', *International Journal of Developmental Biology*, 56(1–3), pp. 83–91. doi: 10.1387/ijdb.113452cg.

González-Estévez, C., Felix, D. A., *et al.* (2012) 'SMG-1 and mTORC1 act antagonistically to regulate response to injury and growth in planarians', *PLoS Genetics*, 8(3). doi: 10.1371/journal.pgen.1002619.

González, A. and Hall, M. N. (2017) 'Nutrient sensing and TOR signaling in yeast and mammals', *The EMBO Journal*. John Wiley & Sons, Ltd, 36(4), pp. 397–408. doi: 10.15252/embj.201696010.

Grohme, M. A. *et al.* (2018) 'The genome of *Schmidtea mediterranea* highlights the plasticity of cellular core mechanisms', *Nature Publishing Group*. Nature Publishing Group, pp. 1–24. doi: 10.1038/nature25473.

Guertin, D. a and Sabatini, D. M. (2006) 'Cell Size Control', *Encyclopedia of Life Sciences*, pp. 1–10. doi: 10.1038/npg.els.0003359.

Hariharan, I. K. (2015) 'Organ Size Control: Lessons from *Drosophila*', *Developmental Cell*. Elsevier Inc., 34(3), pp. 255–265. doi: 10.1016/j.devcel.2015.07.012.

Khalturin, K. *et al.* (2008) 'A novel gene family controls species-specific morphological traits in *Hydra*', *PLoS Biology*. Edited by N. Patel. Public Library of Science, 6(11), pp. 2436–2449. doi: 10.1371/journal.pbio.0060278.

King, R. S. and Newmark, P. A. (2013) 'In situ hybridization protocol for enhanced detection of gene expression in the planarian *Schmidtea mediterranea*.', *BMC developmental biology*, 13(1), p. 8. doi: 10.1186/1471-213X-13-8.

Langmead, B. *et al.* (2009) 'Ultrafast and memory-efficient alignment of short DNA sequences to the human genome', *Genome Biology*. BioMed Central, 10(3), p. R25. doi: 10.1186/gb-2009-10-3-r25.

Li, H. *et al.* (2009) 'The Sequence Alignment/Map format and SAMtools', *Bioinformatics*. Narnia, 25(16), pp. 2078–2079. doi: 10.1093/bioinformatics/btp352.

Lin, A. Y. T. and Pearson, B. J. (2017) 'Yorkie is required to restrict the injury responses in planarians', *PLoS Genetics*, 13(7), pp. 1–30. doi: 10.1371/journal.pgen.1006874.

Lloyd, A. C. (2013) 'The regulation of cell size', *Cell*, p. 1194. doi: 10.1016/j.cell.2013.08.053.

Long, M. *et al.* (2003) 'The origin of new genes: Glimpses from the young and old', *Nature Reviews Genetics*. Nature Publishing Group, pp. 865–875. doi: 10.1038/nrg1204.

Lowe, S. W. and Lin, A. W. (2000) 'Apoptosis in cancer', *Carcinogenesis*. Narnia, pp. 485–495. doi: 10.1093/carcin/21.3.485.

Lupas, A., Van Dyke, M. and Stock, J. (1991) 'Predicting coiled coils from protein sequences', *Science*, 252(5009), pp. 1162–1164. doi: 10.1126/science.252.5009.1162.

März, M., Seebeck, F. and Bartscherer, K. (2013) 'A Pitx transcription factor controls the establishment and maintenance of the serotonergic lineage in planarians.', *Development (Cambridge, England)*,

140(22), pp. 4499–509. doi: 10.1242/dev.100081.

McLysaght, A. and Hurst, L. D. (2016) ‘Open questions in the study of de novo genes: what, how and why.’, *Nature reviews. Genetics*. Nature Publishing Group, 17(9), pp. 567–78. doi: 10.1038/nrg.2016.78.

Miller, C. M. and Newmark, P. a. (2012) ‘An insulin-like peptide regulates size and adult stem cells in planarians’, *International Journal of Developmental Biology*, 56(1–3), pp. 75–82. doi: 10.1387/ijdb.113443cm.

Miyaoka, Y. *et al.* (2012) ‘Hypertrophy and Unconventional Cell Division of Hepatocytes Underlie Liver Regeneration’, *Current Biology*. Elsevier, 22(13), pp. 1166–1175. doi: 10.1016/j.cub.2012.05.016.

Molina, M. D. *et al.* (2011) ‘Noggin and noggin-like genes control dorsoventral axis regeneration in planarians.’, *Current biology : CB*, 21(4), pp. 300–5. doi: 10.1016/j.cub.2011.01.016.

Moritz, S. *et al.* (2012) ‘Heterogeneity of planarian stem cells in the S/G2/M phase.’, *The International journal of developmental biology*, 56(1–3), pp. 117–25. doi: 10.1387/ijdb.113440sm.

Moya, I. M. and Halder, G. (2019) ‘Hippo–YAP/TAZ signalling in organ regeneration and regenerative medicine’, *Nature Reviews Molecular Cell Biology*. Nature Publishing Group, pp. 211–226. doi: 10.1038/s41580-018-0086-y.

Nacu, E. and Tanaka, E. M. (2011) ‘Limb Regeneration: A New Development?’, *Annual Review of Cell and Developmental Biology*. Annual Reviews, 27(1), pp. 409–440. doi: 10.1146/annurev-cellbio-092910-154115.

Neme, R. and Tautz, D. (2013) ‘Phylogenetic patterns of emergence of new genes support a model of frequent de novo evolution’, *BMC Genomics*. BioMed Central, 14(1), p. 117. doi: 10.1186/1471-2164-14-117.

Newmark, P. a and Sánchez Alvarado, a (2000) ‘Bromodeoxyuridine specifically labels the regenerative stem cells of planarians.’, *Developmental biology*, 220(2), pp. 142–53. doi: 10.1006/dbio.2000.9645.

Nowak, K. *et al.* (2013) ‘Nutrient restriction enhances the proliferative potential of cells lacking the tumor suppressor PTEN in mitotic tissues’, *eLife*, 2013(2), pp. 1–21. doi: 10.7554/eLife.00380.

Van Oss, S. B. and Carvunis, A. R. (2019) ‘De novo gene birth’, *PLoS genetics*, 15(5), p. e1008160. doi: 10.1371/journal.pgen.1008160.

Oviedo, N. J. *et al.* (2008) ‘Planarian PTEN homologs regulate stem cells and regeneration through TOR signaling’, *Disease models & mechanisms*, 1(2–3), pp. 131–143. doi: 10.1242/dmm.000117.

Oviedo, N. J., Newmark, P. A. and Sánchez Alvarado, A. (2003) ‘Allometric scaling and proportion regulation in the freshwater planarian *Schmidtea mediterranea*.’, *Developmental dynamics : an official publication of the American Association of Anatomists*, 226(2), pp. 326–33. doi: 10.1002/dvdy.10228.

Palmieri, N., Kosiol, C. and Schlötterer, C. (2014) ‘The life cycle of *Drosophila* orphan genes’, *eLife*, 3. doi: 10.7554/eLife.01311.

Peiris, T. H. *et al.* (2012) ‘TOR signaling regulates planarian stem cells and controls localized and organismal growth’, *Journal of Cell Science*, 125(7), pp. 1657–1665. doi: 10.1242/jcs.104711.

Peiris, T. H. *et al.* (2016) ‘The Akt signaling pathway is required for tissue maintenance and regeneration in planarians’, *BMC Developmental Biology*. BMC Developmental Biology, 16(1), p. 7. doi: 10.1186/s12861-016-0107-z.

Pellettieri, J. *et al.* (2010) ‘Cell death and tissue remodeling in planarian regeneration.’, *Developmental biology*. Elsevier Inc., 338(1), pp. 76–85. doi: 10.1016/j.ydbio.2009.09.015.

Pifferi, F. and Aujard, F. (2019) ‘Caloric restriction, longevity and aging: Recent contributions from human and non-human primate studies’, *Progress in Neuro-Psychopharmacology and Biological Psychiatry*. Elsevier, 95, p. 109702. doi: 10.1016/j.pnpbp.2019.109702.

Pomerantz, J. H. and Blau, H. M. (2013) ‘Tumor suppressors: enhancers or suppressors of regeneration?’, *Development*. The Company of Biologists, 140(12), pp. 2502–2512. doi: 10.1242/dev.084210.

Reinhardt, J. A. *et al.* (2013) ‘De Novo ORFs in *Drosophila* Are Important to Organismal Fitness and

Evolved Rapidly from Previously Non-coding Sequences', *PLoS Genet*, 9(10), p. 1003860. doi: 10.1371/journal.pgen.1003860.

Robinson, J. T. *et al.* (2011) 'Integrative genomics viewer', *Nature Biotechnology*, 29(1), pp. 24–26. doi: 10.1038/nbt.1754.

Ross, K. G. *et al.* (2015) 'Novel monoclonal antibodies to study tissue regeneration in planarians', *BMC Developmental Biology*, 15. doi: 10.1186/s12861-014-0050-9.

Salazar-Roa, M. and Malumbres, M. (2017) 'Fueling the Cell Division Cycle', *Trends in Cell Biology*. Elsevier, pp. 69–81. doi: 10.1016/j.tcb.2016.08.009.

Sanchez Alvarado, A. and Newmark, P. A. (1999) 'Double-stranded RNA specifically disrupts gene expression during planarian regeneration', *Proceedings of the National Academy of Sciences*, 96(9), pp. 5049–5054. doi: 10.1073/pnas.96.9.5049.

Saxton, R. A. and Sabatini, D. M. (2017) 'mTOR Signaling in Growth, Metabolism, and Disease', *Cell*. Cell Press, pp. 960–976. doi: 10.1016/j.cell.2017.02.004.

Schlötterer, C. (2015) 'Genes from scratch - the evolutionary fate of de novo genes', *Trends in Genetics*, 31(4), pp. 215–219. doi: 10.1016/j.tig.2015.02.007.

Solana, J. *et al.* (2012) 'Defining the molecular profile of planarian pluripotent stem cells using a combinatorial RNAseq, RNA interference and irradiation approach.', *Genome biology*, 13(3), p. R19. Available at: <http://genomebiology.com/content/pdf/gb-2012-13-3-r19.pdf> (Accessed: 4 September 2019).

de Sousa, N. *et al.* (2018) 'Hippo signaling controls cell cycle and restricts cell plasticity in planarians', *PLoS Biology*, 16(1). doi: 10.1371/journal.pbio.2002399.

Sureda-Gómez, M., Martín-Durán, J. M. and Adell, T. (2016) 'Localization of planarian β CATENIN-1 reveals multiple roles during anterior-posterior regeneration and organogenesis', *Development*, (October), p. dev.135152. doi: 10.1242/dev.135152.

Tautz, D. and Domazet-Lošo, T. (2011) 'The evolutionary origin of orphan genes', *Nature Reviews Genetics*. Nature Publishing Group, pp. 692–702. doi: 10.1038/nrg3053.

Thommen, A. *et al.* (2019) 'Body size-dependent energy storage causes Kleiber's law scaling of the metabolic rate in planarians', *eLife*, 8, pp. 1–29. doi: 10.7554/eLife.38187.

Toll-Riera, M. *et al.* (2009) 'Origin of primate orphan genes: A comparative genomics approach', *Molecular Biology and Evolution*. Narnia, 26(3), pp. 603–612. doi: 10.1093/molbev/msn281.

Trifinopoulos, J. *et al.* (2016) 'W-IQ-TREE: a fast online phylogenetic tool for maximum likelihood analysis', *Nucleic Acids Research*. Narnia, 44(W1), pp. W232–W235. doi: 10.1093/nar/gkw256.

Tu, K. C., Pearson, B. J. and Sánchez Alvarado, A. (2012) 'TORC1 is required to balance cell proliferation and cell death in planarians', *Developmental Biology*. Elsevier Inc., 365(2), pp. 458–469. doi: 10.1016/j.ydbio.2012.03.010.

Tumaneng, K. *et al.* (2012) 'YAP mediates crosstalk between the Hippo and PI(3)K-TOR pathways by suppressing PTEN via miR-29', *Nature Cell Biology*. Nature Publishing Group, 14(12), pp. 1322–1329. doi: 10.1038/ncb2615.

Udan, R. S. *et al.* (2003) 'Hippo promotes proliferation arrest and apoptosis in the Salvador/Warts pathway', *Nature Cell Biology*, 5(10), pp. 914–920. doi: 10.1038/ncb1050.

Waterhouse, A. M. *et al.* (2009) 'Jalview Version 2--a multiple sequence alignment editor and analysis workbench', *Bioinformatics*. Narnia, 25(9), pp. 1189–1191. doi: 10.1093/bioinformatics/btp033.

Wenemoser, D. *et al.* (2012) 'A molecular wound response program associated with regeneration initiation in planarians.', *Genes & development*, 26(9), pp. 988–1002. doi: 10.1101/gad.187377.112.

Wenemoser, D. and Reddien, P. W. (2010) 'Planarian regeneration involves distinct stem cell responses to wounds and tissue absence.', *Developmental biology*, 344(2), pp. 979–991. doi: 10.1016/j.ydbio.2010.06.017.

Werner, M. S. *et al.* (2018) 'Young genes have distinct gene structure , epigenetic profiles , and transcriptional regulation Department of Evolutionary Biology , Max Planck Institute for Developmental Biology , Keywords':, *Genome Research*, 28, pp. 1675–1687. doi: 10.1101/gr.234872.118.

- Willsey, H. R. *et al.* (2016) 'Localized JNK signaling regulates organ size during development', *eLife*, 5(MARCH2016), pp. 1–18. doi: 10.7554/eLife.11491.
- Wilson, B. A. *et al.* (2017) 'Young genes are highly disordered as predicted by the preadaptation hypothesis of de novo gene birth', *Nature Ecology and Evolution*, 1(6). doi: 10.1038/s41559-017-0146.
- Wilson, G. A. *et al.* (2005) 'Orphans as taxonomically restricted and ecologically important genes', *Microbiology*, pp. 2499–2501. doi: 10.1099/mic.0.28146-0.
- Wolfson, R. L. and Sabatini, D. M. (2017) 'The Dawn of the Age of Amino Acid Sensors for the mTORC1 Pathway', *Cell Metabolism*, pp. 301–309. doi: 10.1016/j.cmet.2017.07.001.
- Yoon, M. S. (2017) 'The role of mammalian target of rapamycin (mTOR) in insulin signaling', *Nutrients*, 9(11). doi: 10.3390/nu9111176.
- Zeng, Q. and Hong, W. (2008) 'The Emerging Role of the Hippo Pathway in Cell Contact Inhibition, Organ Size Control, and Cancer Development in Mammals', *Cancer Cell*, pp. 188–192. doi: 10.1016/j.ccr.2008.02.011.
- Zhao, L. *et al.* (2014) 'Origin and spread of de novo genes in *Drosophila melanogaster* populations', *Science*, 343(6172), pp. 769–772. doi: 10.1126/science.1248286.

Figures

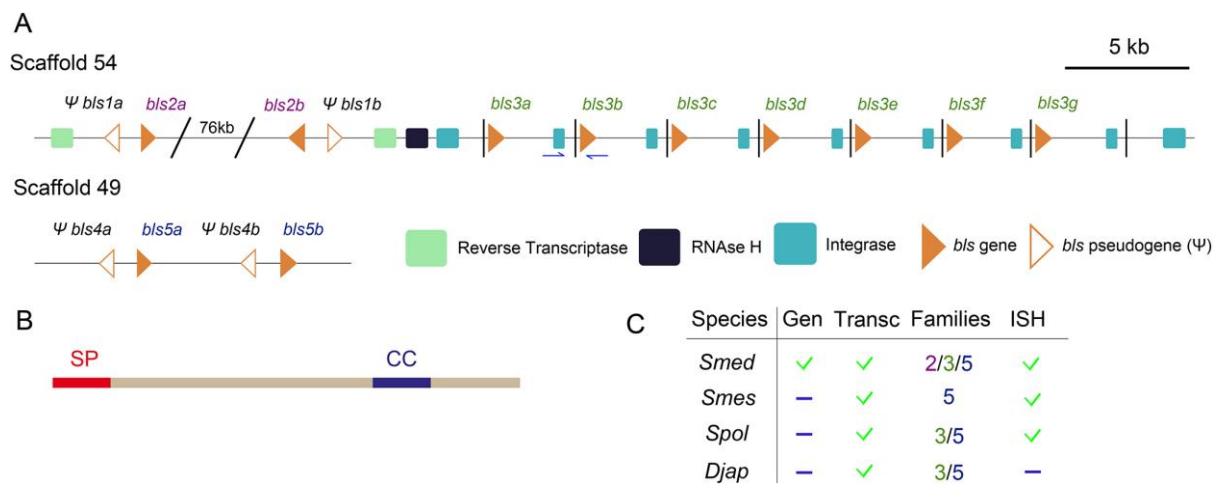


Figure 1. The *bls* family is composed of 11 genes and 4 pseudogenes. (A) Cartoon illustrating the genomic organization of *Bls* family members. Subfamilies *bls1*, *bls2*, and *bls3* are found in scaffold 54 and subfamilies *bls4* and *bls5* in scaffold 49. Primers used to amplify the junction of the first *bls3* repeats are indicated in blue. *bls* genes are represented with orange triangles. *bls* pseudogenes (Ψ) are represented with white and orange triangles. Transposon elements are indicated with squares. Scale bar indicates base pairs. (B) *Bls* protein domains: red, signal peptide (SP); blue, coiled coil (CC). (C) *bls* homologs found in the available genomic (Gen) and transcriptomic (Transc) datasets for planarian species. Expression as detected by ISH is indicated. Green check indicates presence of *bls* homolog; blue line indicates no available data. ISH, *in situ* hybridization; *Smed*, *Schmidtea mediterranea* (asexual strain); *Smes*, *Schmidtea mediterranea* (sexual strain); *Spol*, *Schmidtea polychroa*; *Djap*, *Dugesia japonica*.

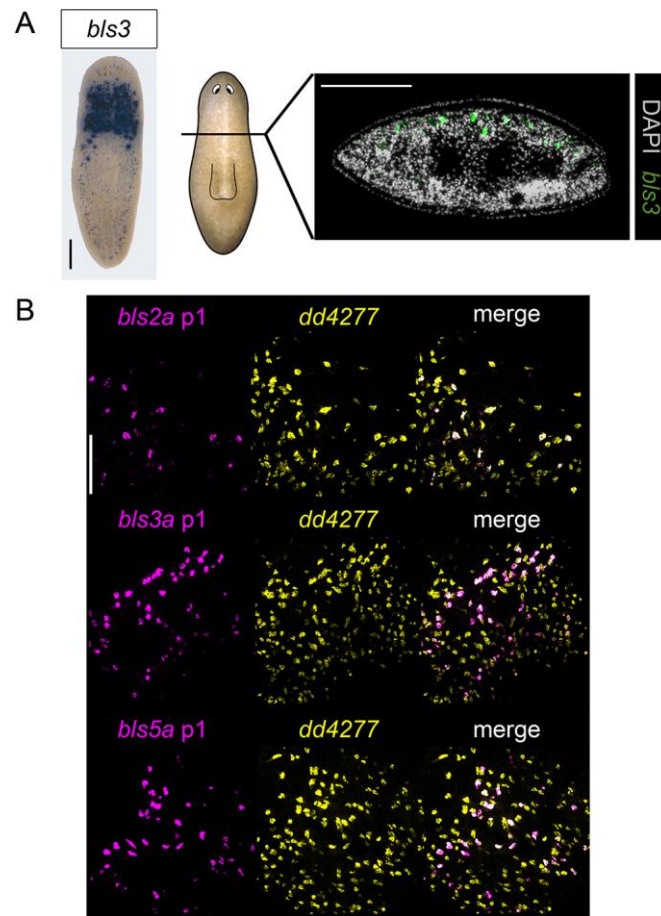


Figure 2. *bls* expression pattern. (A) *bls3* expression in a transverse section as detected by WISH (blue) and FISH (green). Nuclei are stained with DAPI. (B) *bls2*, *bls3* and *bls5* co-expression with *dd4277*. Scale bars: 200 μ m in A and B.

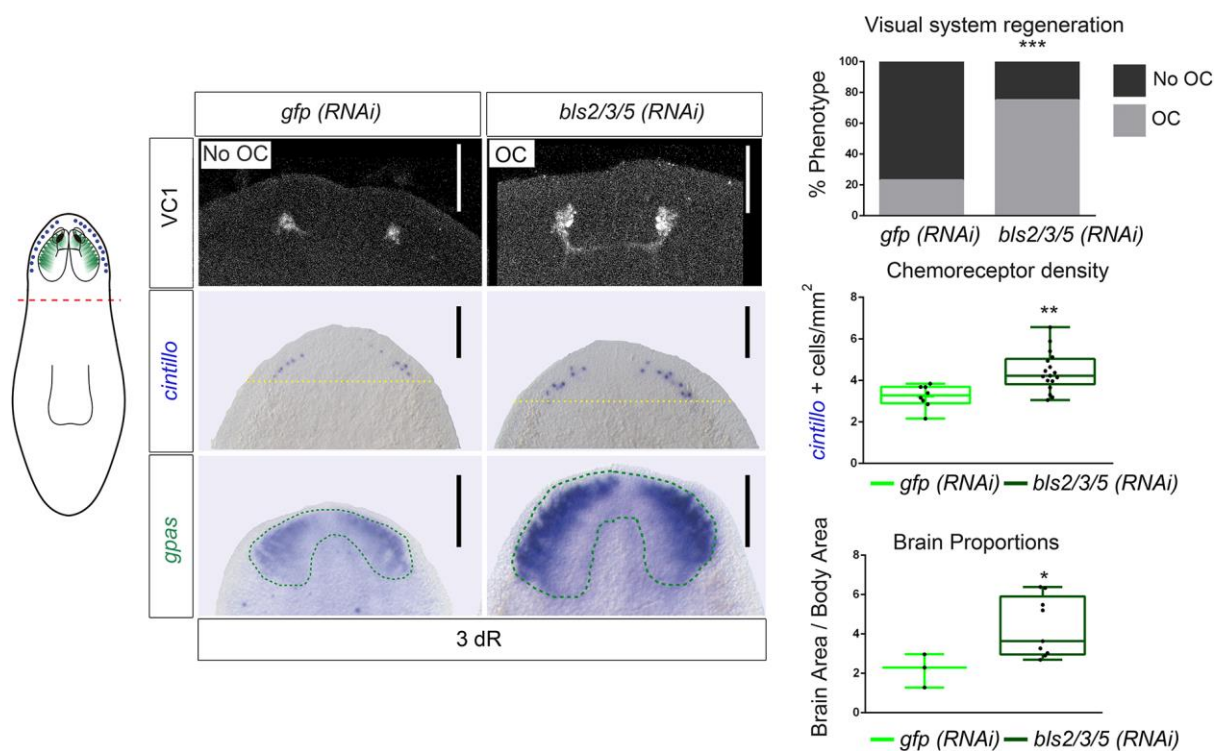


Figure 3. Regeneration is accelerated in *bls2/3/5* RNAi planarians. Immunohistochemistry with anti-arrestin antibody (VC1), labelling the visual system; WISH showing *cintillo* (chemoreceptors) and *gas* (brain branches) expression. Illustration indicates areas of *gas* and *cintillo* expression and positive arrestin (VC1) staining; dashed red line represents the level at which amputation was performed. Images show quantification of the appearance of the optic chiasm (controls, n=23; RNAi, n=23; *** $P < 0.001$), *cintillo*+ cells/mm² (the area quantified is indicated with a yellow dashed line) (controls, n=8; RNAi, n=17, ** $P < 0.01$), and *gas*+ area/body area (*gas*+ area is indicated with a green dashed line) (controls, n=3; RNAi, n=9 ; * $P < 0.05$) in *gfp*(RNAi) and *bls2/3/5*(RNAi) animals at 3 days of regeneration (3 dR). Scale bars: 100 μ m.

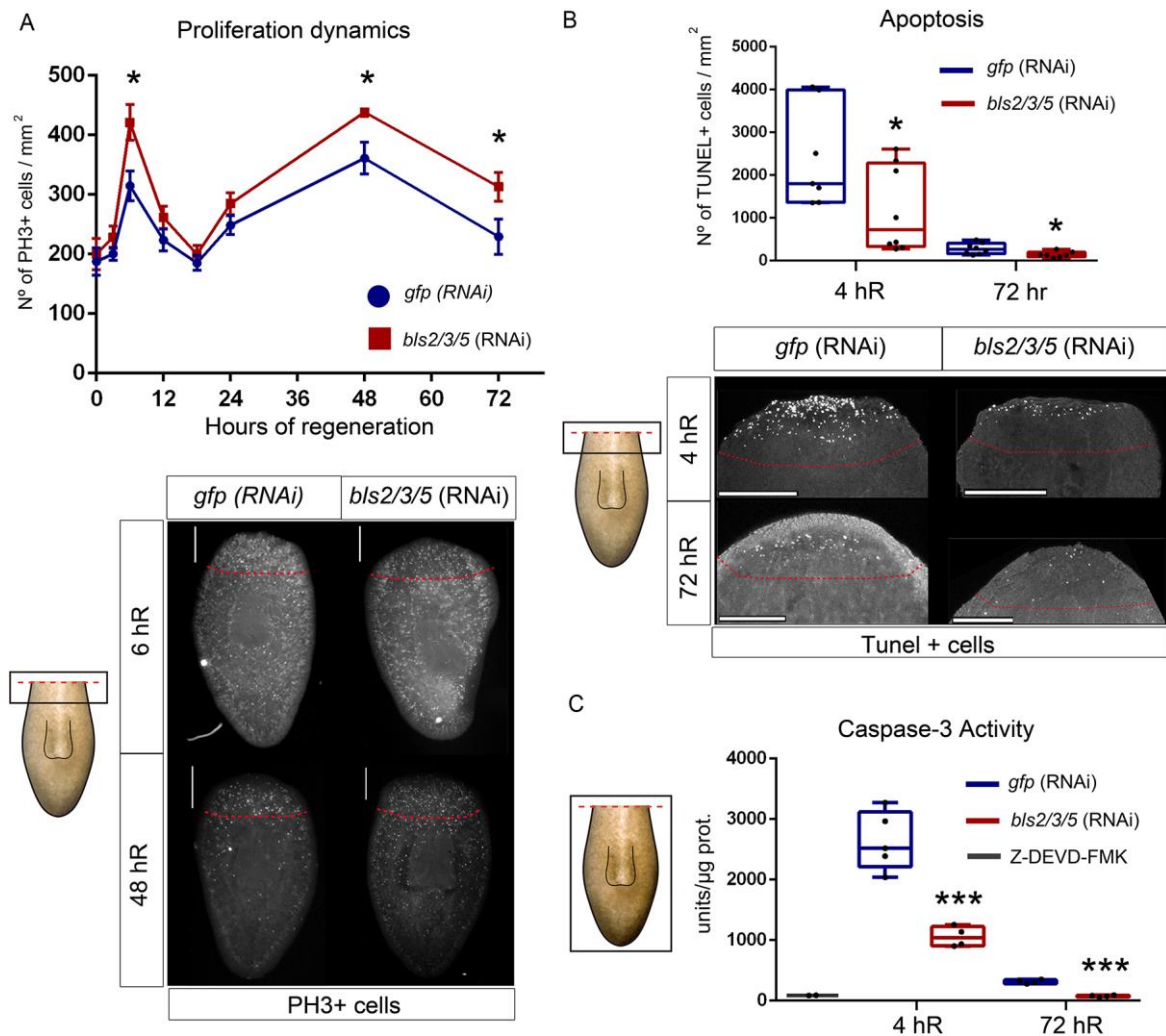


Figure 4. After *bls2/3/5* RNAi planarians exhibit increased proliferation and decreased apoptosis during anterior regeneration. (A) Quantification of PH3+ cells at different stages of regeneration (controls, n>5; RNAi, n>5; * P <0.05). Lower panel shows anti-PH3 immunostaining of *gfp*(RNAi) and *bls2/3/5*(RNAi) animals. (B) Quantification of TUNEL+ cells in *bls2/3/5*(RNAi) and control animals (controls, n>7; RNAi, n>7; * P <0.05). Lower panel shows TUNEL images. Images correspond to Z projections. (C) Quantification of caspase-3 activity in *bls2/3/5*(RNAi) animals and controls (controls, n=4; RNAi, n=4; *** P <0.001). In the schematic drawing red dashed line represents the amputation plane and the square indicates the region analyzed. In the images the red dashed line limits the area quantified. Scale bars: 500 μ m (A) and 200 μ m (B).

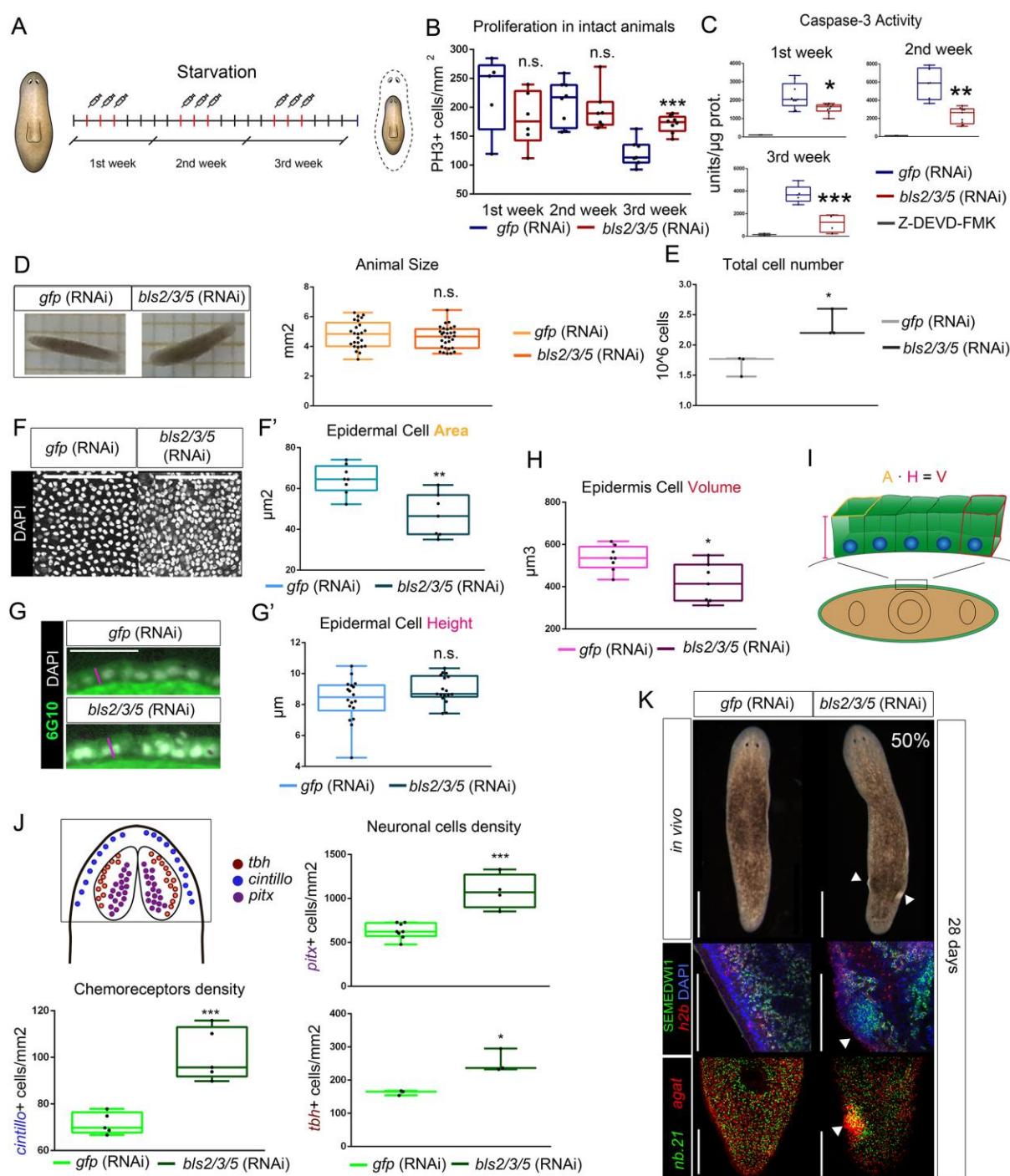


Figure 5. In starving conditions, *bls2/3/5*(RNAi) animals show decreased cell death and cell accumulation but not an increase in body size. (A) Schematic depicting RNAi procedure. (B) Quantification of PH3+ cells after one week of RNAi treatment (controls, n=5; RNAi, n=6; n.s.); two weeks of RNAi treatment (controls, n=7; RNAi, n=6; n.s.); and 3 weeks of RNAi treatment (controls, n=7; RNAi, n=9; ****P*<0.001). Quantification is based in the number of PH3+ cells per body area (C) Quantification of caspase-3 after one week of RNAi treatment (controls, n=9; RNAi, n=9; **P*<0.05); two

weeks of treatment (controls, n=6; RNAi, n=9; ** $P<0.01$); and 3 weeks of treatment (controls, n=10; RNAi, n=8; *** $P<0.001$). (D) Quantification of body area in vivo animals (controls, n=25; RNAi, n=30; n.s.). (E) Quantification of cell number (controls, n=3; RNAi, n=3; * $P<0.05$). Each biological replicate represents 5 animals. (F) DAPI staining of epithelial cells of the prepharyngeal region. (F') Quantification of the mean epidermal cell area (A) (controls, n=8; RNAi, n=7; ** $P<0.01$). (G) Transverse sections of planarian epidermis immunostained with anti-6G10. The distance from the basal to the apical part of the cells (epidermal cell height, H) is indicated with a pink line. (G') Height quantification (controls, n=18, RNAi, n=17, n.s.). (H) Quantification of epidermal cell volume (V) (controls, n=8; RNAi, n=7; * $P<0.05$). (I) Schematic illustration of the measurements performed to quantify V. (J) Illustration depicts the expression of *cintillo*, *pitx*, and *tbh*. The square indicates the area quantified. Quantification of *cintillo*+ cells/head area (controls, n=5; RNAi, n=5; *** $P<0.001$), *pitx*+ cells/head area (controls, n=8; RNAi, n=4; *** $P<0.001$), *tbh*+ cells/head area (controls, n=3; RNAi, n=3; * $P<0.05$). (K) 50% of animals developed overgrowths after 4 weeks of *bls2/3/5* inhibition in starved conditions. FISH of *h2b* riboprobe combined with anti-SMEDWI-1 immunostaining, and FISH with *agat+* and *nb.21* riboprobes (controls, n=60; RNAi, n=58). White arrows indicate overgrowths. Images from F and K correspond to Z projections. Scale bars: one side of a square = to 1 mm (D), 20 μm (F and G), or 500 μm (K).

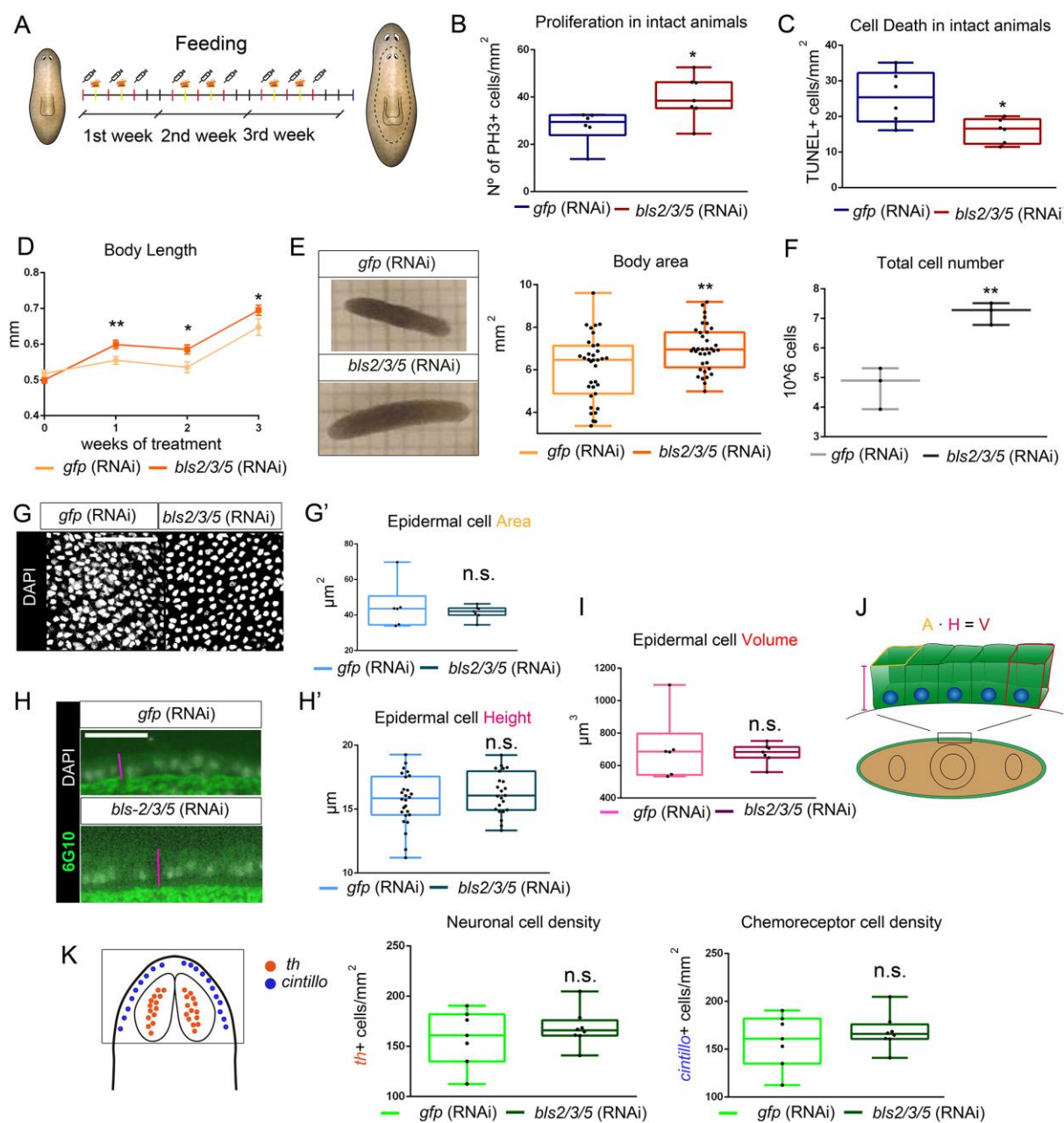


Figure 6. In fed conditions, *bls2/3/5*(RNAi) animals show an increase in proliferation and a decrease in cell death, which results in larger animals. (A) Schematic depicting the RNAi procedure (B) Quantification of PH3+ cells after 3 weeks of RNAi treatment (controls, n=6; RNAi, n=7; *P<0.05). Quantification is based in the number of PH3+ cells per body area (C) Quantification of TUNEL+ cells after 3 weeks of RNAi treatment (controls, n=6; RNAi, n=6; *P<0.05) (see materials and methods and Fig. S6E for details of quantification). (D) Length of control and RNAi animals (controls, n >35; RNAi, n >35; *P<0.05, **P<0.01). (E) Quantification of body area in live animals (controls, n=35; RNAi, n=36; **P<0.01). (F) Quantification of cell number (controls, n=3; RNAi, n=3; **P<0.01). Each biological replicate represents 5 animals. (G) DAPI staining of epithelial cells of the prepharyngeal region. (G')

Quantification of mean epidermal cell area (A) (controls, n=6; RNAi, n=7; n.s.). (H) Transverse sections of planarian epidermis immunostained with anti-6G10. The distance from the basal to the apical part of the cell (epidermal cell height, H) is indicated with a pink line. (H') Quantification of H (controls, n=26; RNAi, n=23; n.s.). (I) Quantification of epidermal cell volume (V) (controls, n=6; RNAi, n=7; n.s.). (J) Illustration showing measurements used to quantify V. (K) Quantification of *th*⁺ cells/head area (controls, n=9; RNAi, n=6; n.s.) and *cintillo*⁺ cells/head area (controls, n=7; RNAi, n=8; n.s.). Illustration depicts the expression of *th* and *cintillo*, and the square indicates the area quantified. Images from G' correspond to Z projections. Scale bars: one side of a square = 1 mm (D') or 20 μm (G and H).

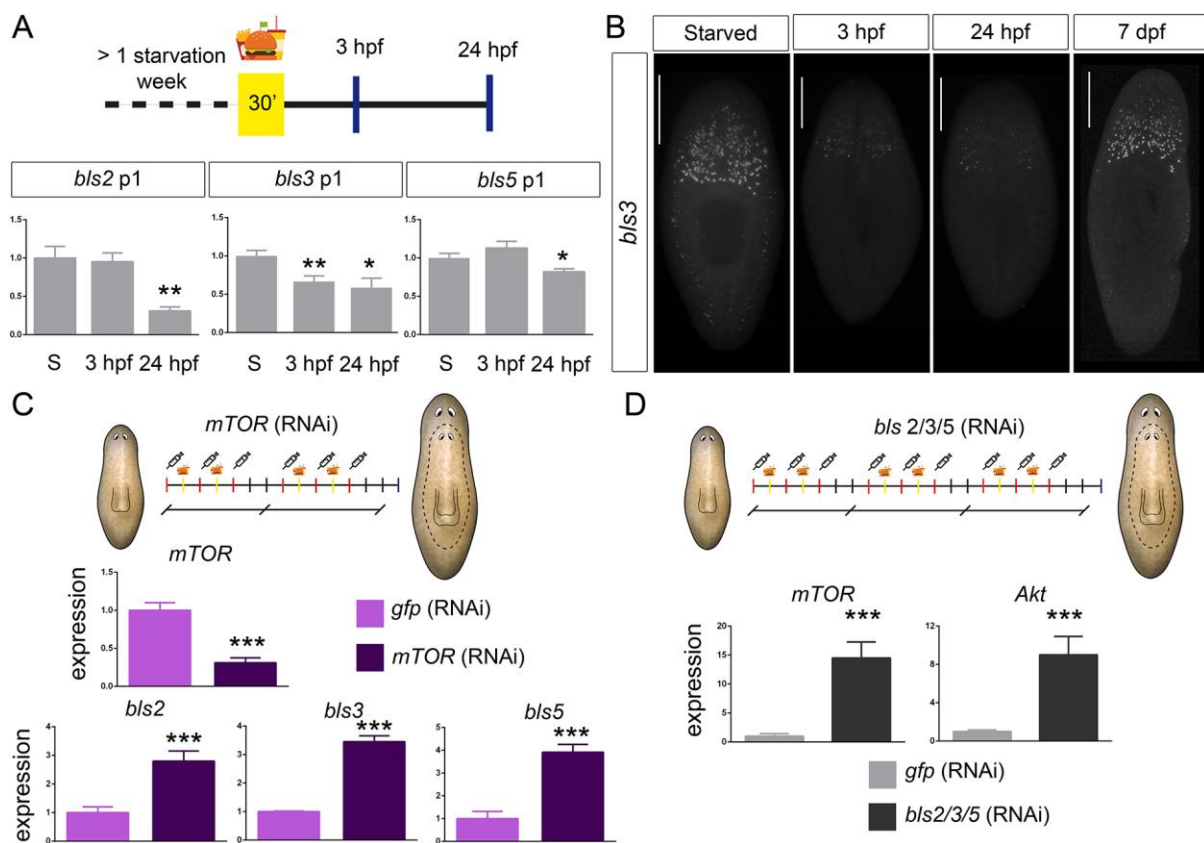


Figure 7. *bls2*, *bls3*, and *bls5* levels are regulated by food ingestion and by mTOR signalling (A) Schematic depicting the experimental procedure. Animals were starved for more than 1 week and then fed for 30 minutes and fixed at different time points thereafter. Bar charts represent qRT-PCR quantification of *bls2*, *bls3*, and *bls5* expression in starved animals (S) and in fed animals 3 and 24 hours post-feeding (hpf). (B) Representative FISH images of *bls3* before feeding and at different time points after feeding, demonstrating its reduced expression at 3 hpf and 24 hpf, and its recovery at 7 dpf. (C) qRT-PCR quantification of *bls2*, *bls3*, and *bls5* expression in fed *mTOR* (RNAi) animals. Scheme depicts the RNAi procedure. (D) qRT-PCR quantification of *mTOR* and *Akt* expression in fed *bls2/3/5* (RNAi) animals. Scheme depicts the RNAi procedure. In all the panel, relative expression is plotted as $2^{-\Delta\Delta CT}$ values. Data represent the mean and s.d. (bars). * $P < 0.05$; ** $P < 0.01$, *** $P < 0.001$

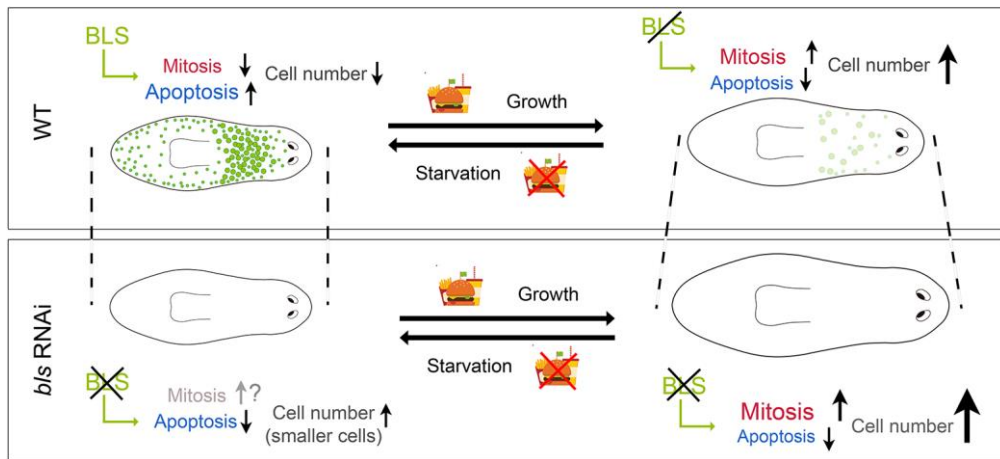


Figure 8. Model representing *bIs*-mediated control of cell number. In starving conditions *bIs* is expressed and limits cell number and body size by promoting apoptosis without significantly affecting mitotic index. After feeding *bIs* is down-regulated, allowing an increase in mitotic cells and a decrease in cell death, which results in an increase in cell number. In starved *bIs* RNAi animals the mitosis:apoptosis ratio increases, as does total cell number. However, cells cannot maintain their size and body size does not increase. In fed *bIs* RNAi animals, the mitosis:apoptosis ratio is even higher than in controls and cell number increases. This is accompanied by an increase in body size, since cells maintain their normal size.

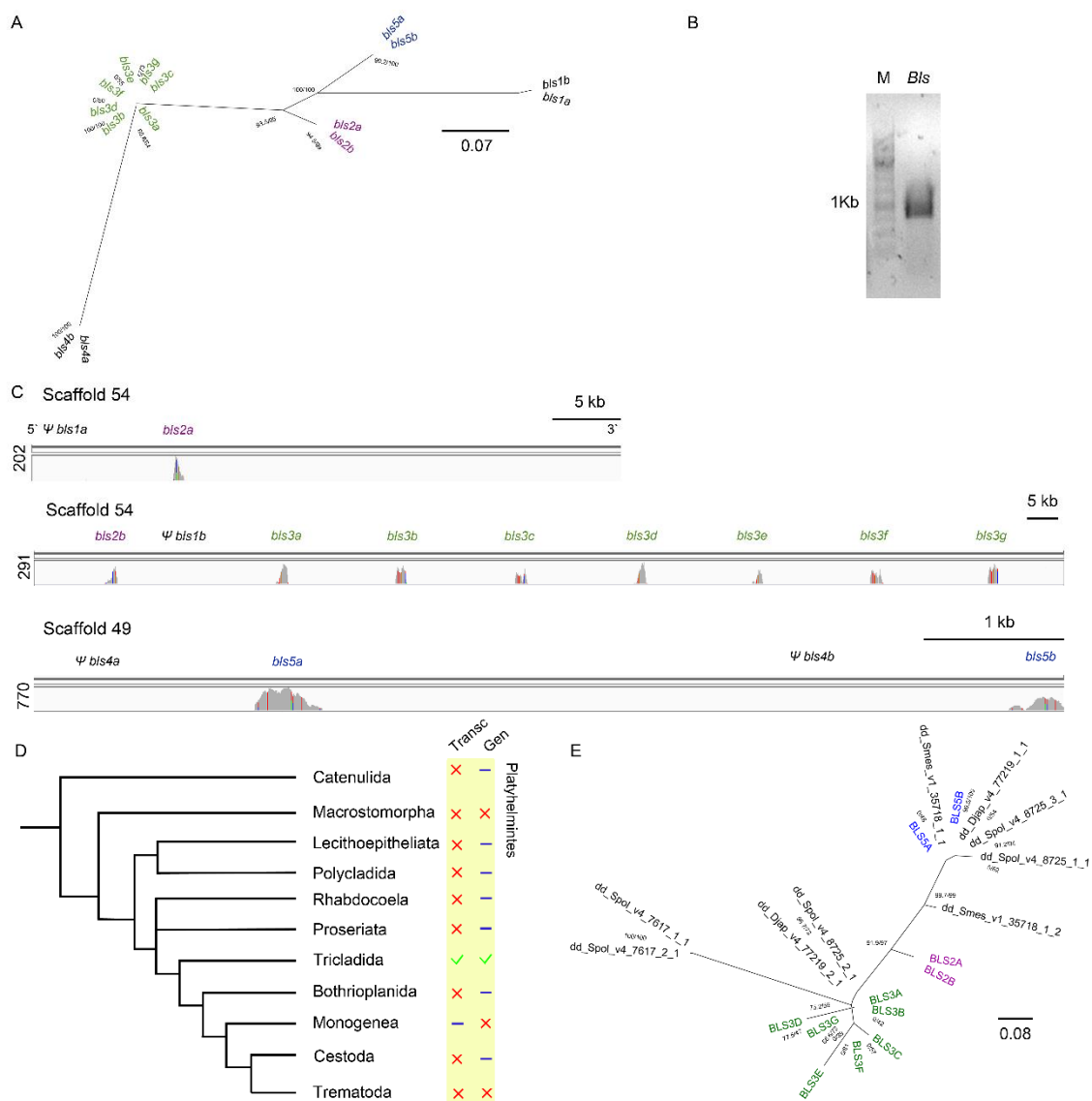


Figure S1. Genomic and evolutionary features of bls subfamilies. (A) Phylogenetic analysis of all members of *Smed* *Bls* family using nucleotide sequences. They group into 5 subfamilies. Scale indicates expected nucleotide substitution per site. (B) PCR analysis using primers flanking the junction of the first bls3 repeat (between bls3a and b) showing the expected 1 Kb band. (C) Transcriptomic reads mapping in the three non-consecutive parts of the two scaffolds where *bls* genes are located. Peaks represent reads accumulation. The absence of peaks is considered a lack of expression. Lateral number represents the higher summit in each track. (D) Presence of *bls* homologs in the transcriptomic (Transc) and genomic (Gen) available databases from different Platyhelminth species. Green check means that presence of some homolog, red cross indicates that no homologs have been identified and blue line indicates no available data. (E) Phylogenetic tree of the *bls* homologs in the Tricladida Order using amino acidic sequences. bls5 subfamily is present in all species, bls3 was not found in *Smes*, and bls2 was only found in *Smed*. Scale indicates expected amino acidic substitution per site.

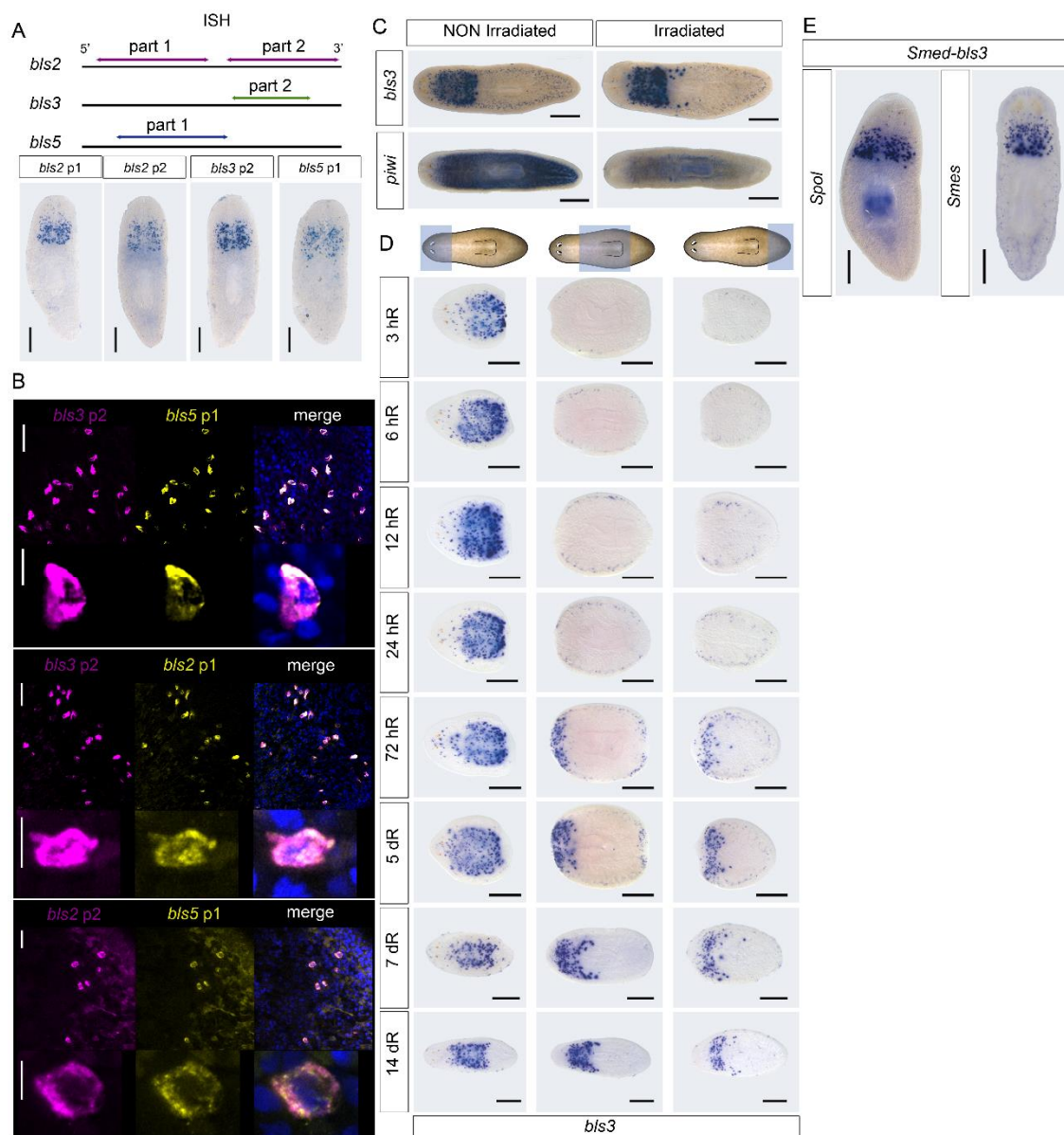


Figure S2. *bls2/3/5* expression in intact and regenerating animals. (A) Scheme indicating the riboprobes designed for each gene family. WISH with the different riboprobes in intact animals showing the similar expression pattern. (B) Double FISH combining all specific riboprobes. Each panel represents each gene combination. A magnification is also shown. All riboprobes colocalize in most of the cells, and magnifications demonstrate that riboprobes present a different cellular distribution. (C) WISH of *bls3* and *piwi* in non-irradiated and irradiated animals. After irradiation the neoblast marker (*piwi*) expression decreases but not *bls3*, corroborating that *bls* gene family are localized in differentiated cells. (D) WISH of *bls3* during regeneration at different time points. From 3hR to 24hR no *bls3* expression is observed in the blastemas. From 72hR to 14dR the new expression and redistribution of *bls3* is observed. (E) WISH of *bls3* in *Schmidtea polychroa* (*Spol*) and *Schmidtea mediterranea* sexual strain (*Smes*), showing the same expression pattern than in *Smed*. Scale bars: A, C, D and E are 500 μ m. In B are 50 μ m and 10 μ m in magnifications.

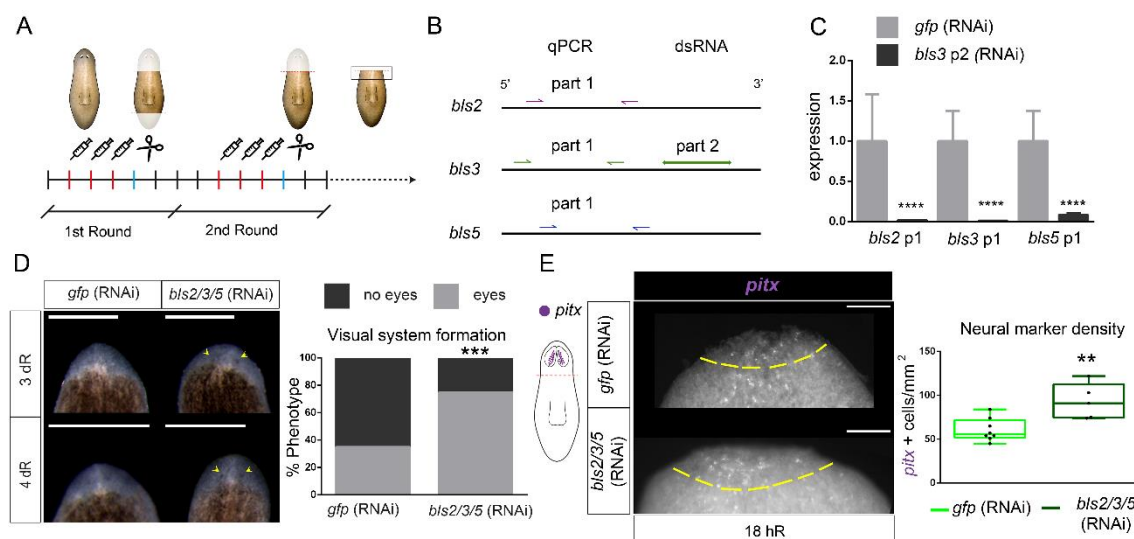


Figure S3. *bls2/3/5* inhibition after RNAi during regeneration, and faster regeneration of *bls2/3/5* (RNAi) animals. (A) Cartoon illustrating the protocol of RNAi inhibition during planarians regeneration. One week starved planarians were injected 3 consecutive days and amputated the following day. The following 3 days, planarians were let to regenerate. Planarians were amputated anterior and posteriorly, and a second week of inhibition was performed only with trunk fragments. The second week trunks were amputated just anteriorly. (B) Scheme indicating the fragments used for RNAi and qPCR analysis. (C) qRT-PCR analysis quantifying *bls2*, *bls3* and *bls5* expression after *bls3* inhibition at 3dR, demonstrating that all three subfamilies were down-regulated after injection of *bls3* dsRNA. Relative expression is plotted as 2^{-CT} values. Data are plotted as mean and error bars represent s. d. (**** $P < 0.0001$). (D) *in vivo* images of planarians showing that in *bls2/3/5* (RNAi) animals regenerating eyes are more evident (yellow arrows) than in controls at 3 and 4dR (n of controls=23, n of RNAi=23, *** $P < 0.001$). (E) Representation of *pitx* expression in *wt* animals. In the drawing, red dashed line represents amputation level. FISH of *pitx* shows an increase of *pitx*+ cells in the blastema at 18 hR. Quantification of *pitx*+ cells / mm^2 is showed (n of controls=8, n of RNAi=5, ** $P < 0.01$). Yellow dashed line in the images indicates the area quantified. Scale bars: 250 μm in (D), 100 μm in (E).

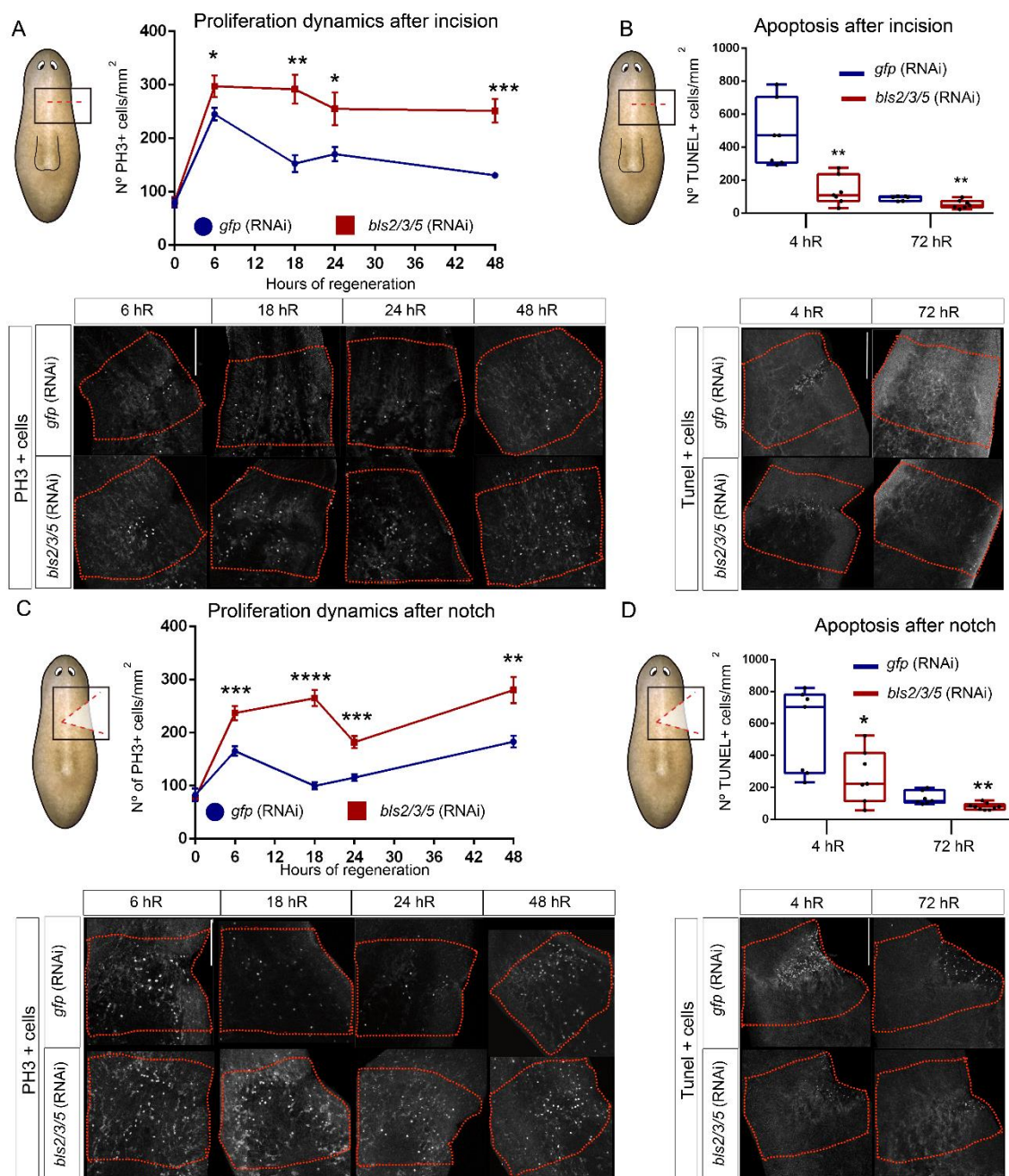


Figure S4. *bIs2/3/5* (RNAi) animals show an increase in proliferation and a decrease of apoptosis after any injury. (A) Quantification of PH3+ cells at different time points after incision shows an increment of mitotic cells/mm² in *bIs2/3/5* (RNAi) animals. Time points were 6 hR (n of controls=5, n of RNAi=7, **P*<0.05), 18 hR (n of controls=6, n of RNAi=7, ***P*<0.01), 24 hR (n of controls=6, n of RNAi=8, **P*<0.05) and 48 hR (n of controls=8, n of RNAi=8, ****P*<0.001). anti-PH3 immunostaining images are shown below. (B) Quantification of TUNEL+ cells show a decrease of apoptotic cells in *bIs2/3/5* (RNAi) animals after incision at 4 hR (n of controls=7, n of RNAi=7, ***P*<0.01) and 72 hR (n of controls=6, n of RNAi=7, ***P*<0.01). TUNEL images are shown below. (C) Quantification of PH3+ cells at different time points after notching shows an

increment of mitotic cells/mm² in *bls2/3/5* (RNAi) animals at 6 hR (n of controls=8, n of RNAi=9, *** $P<0.001$), 18 hR (n of controls=8, n of RNAi=8, **** $P<0.0001$), 24 hR (n of controls=8, n of RNAi=9, *** $P<0.001$) and 48 hR (n of controls=8, n of RNAi=8, ** $P<0.01$). anti-PH3 immunostaining images are shown below. D) Quantification of TUNEL+ cells show a decrease of apoptotic cells in *bls2/3/5* (RNAi) animals after notching at 4 hR (n of controls=7, n of RNAi=7, * $P<0.05$) and 72 hR (n of controls=7, n of RNAi=9, ** $P<0.01$). TUNEL images are shown below. All images correspond to Z projections. Illustrations show the amputation plane and the area analyzed (dashed red line and black square, respectively). Red dashed line in the images indicate the area analyzed. Scale bars: 200 μ m in all panels.

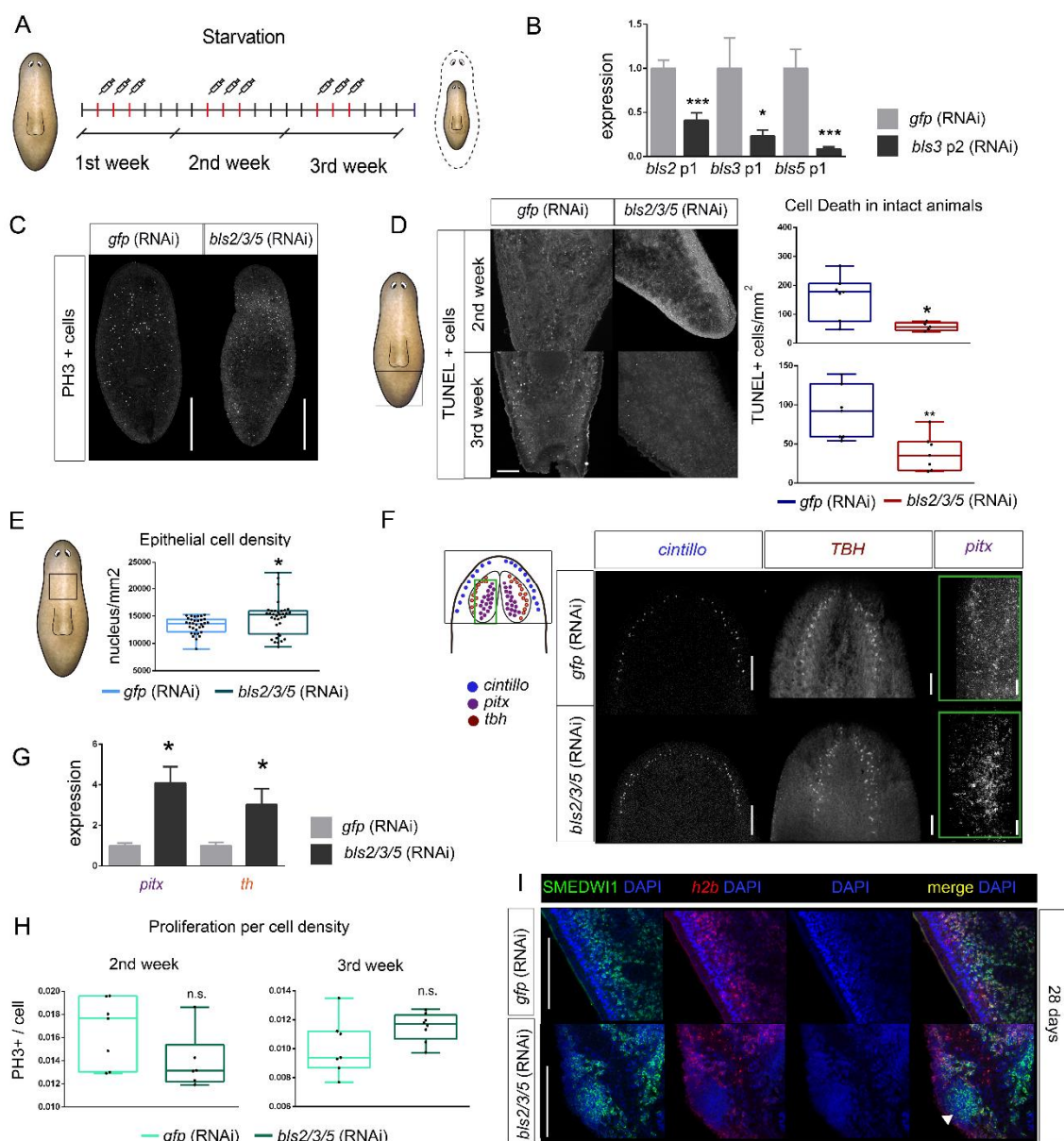


Figure S5. In starved conditions, *bls2/3/5* (RNAi) animals show a decrease in cell death, which leads to cell accumulation and overgrowth formation. (A) Scheme of the RNAi procedure to inhibit *bls2/3/5* in starved planarians. Each week, animals were injected 3 consecutive days. At the end of the third week, animals were fixed and analyzed. (B) qRT-PCR analysis measuring *bls2*, *bls3* and *bls5* expression after 3 weeks of *bls3 p2* inhibition demonstrated that all three genes are down-regulated. Relative expression is plotted as 2^{-CT} values. Data is plotted as mean and error bars represent s.d. (*P<0.05; ***P<0.001). (C) anti-PH3 immunostaining images of *bls2/3/5* (RNAi) animals and controls (D) TUNEL assay images of *bls2/3/5* RNAi animals and controls, corresponding to the posterior region of the animals, which was the area quantified (indicated with a square in the schematic drawing). Images correspond to Z projections after the second and the third week of treatment. Quantification of TUNEL+

cells /area in *bls2/3/5*(RNAi) and control animals; after the second week of treatment (controls, n=7; RNAi, n=5, * $P < 0.05$); and after the third week of treatment (controls, n=7; RNAi, n=7, ** $P < 0.01$). (E) Quantification of Nuclei of epidermal cells stained with DAPI per area (n of controls=15, n of RNAi=15, * $P < 0.05$). The illustration indicates the area quantified with a black square. (F) Confocal images of the expression of neural (*tbh* and *pitx*) and chemoreceptor (*cintillo*) markers in *bls2/3/5* (RNAi) animals and controls. The illustration shows the expression of *tbh*, *pitx* and *cintillo*. *Cintillo* and *tbh*+ cells were quantified with respect to the head area (indicated with a square in the schematic drawing). *pitx*+ cells were quantified in a region of the head (green square in the images). (G) qRT-PCR quantification of the expression of neural markers (*pitx* and *th*). Relative expression is plotted as 2^{-CT} values. Data is plotted as mean and error bars represent s.d. (* $P < 0.05$). (H) Normalization of PH3+cells/area by epidermal cell density (quantified as showed in E) in *bls2/3/5*(RNAi) and control animals. After 2 weeks of RNAi treatment (controls, n=7; RNAi, n=6; n.s.) and 3 weeks of RNAi treatment (controls, n=7; RNAi, n=8; n.s.). (I) Overgrowths of *bls2/3/5*(RNAi) stained with anti-SMEDWI and *h2b* riboprobe. Nuclei are in blue. White arrows indicate overgrowths. Images from D, G and I correspond to Z projections. Scale bars: 500 μm in (C), 100 μm in (D), 200 μm in (G) and 500 μm in (I).

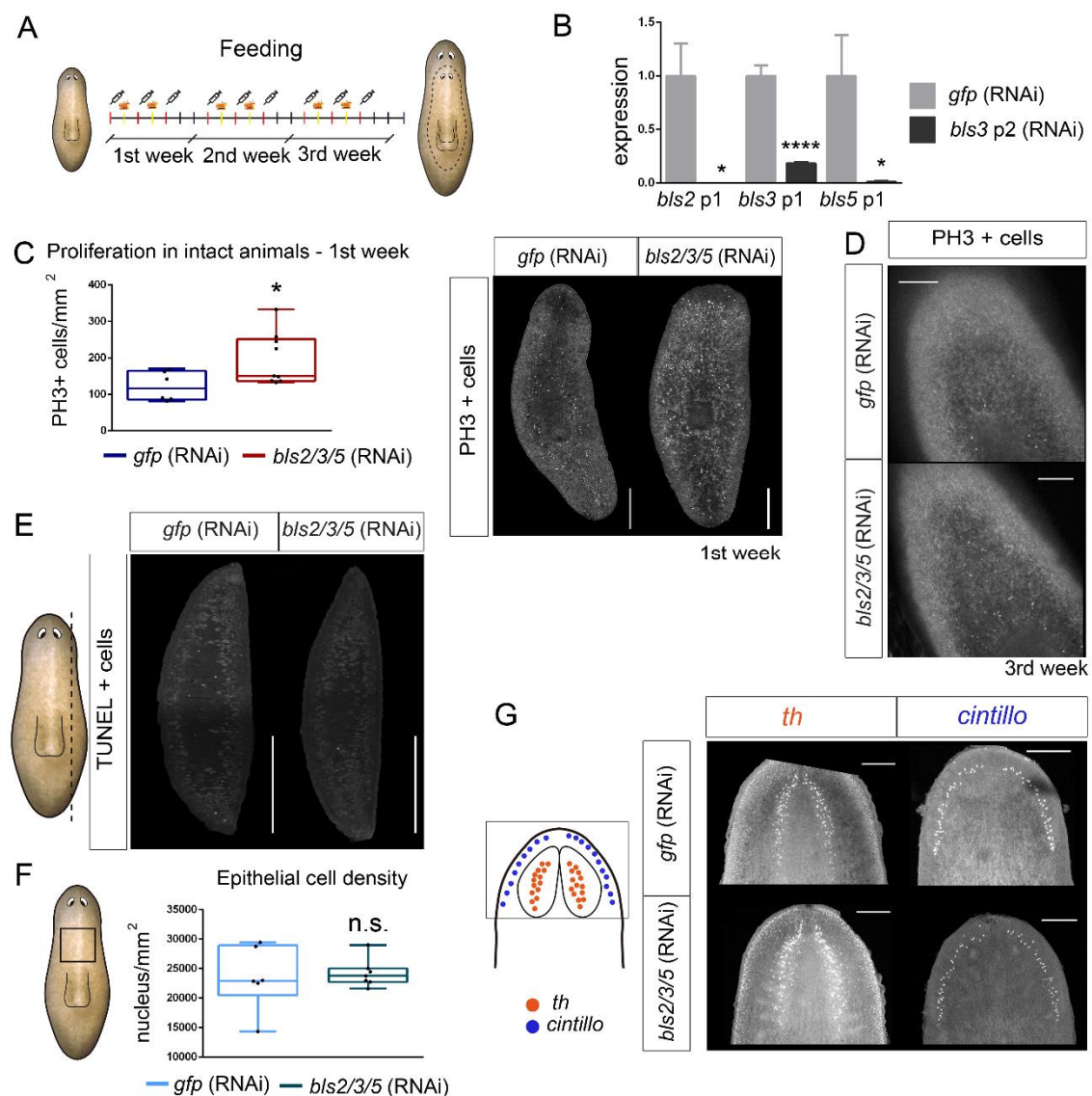


Figure S6. *Bls* inhibition during growth conditions decreases cell proliferation and increases cell death, but does not promote cell accumulation. (A) Scheme of the RNAi procedure to inhibit *bls2/3/5* in fed planarians. Each week, animals were injected 3 non consecutive days, being feed the other two days. At the end of the third week, animals were fixed (three days after the last injection) and analyzed. (B) qRT-PCR quantifying *bls2*, *bls3* and *bls5* expression after 3 rounds of *bls3* inhibition, demonstrating that all three genes are downregulated. Relative expression is plotted as 2^{-CT} values. Data is plotted as mean and error bars represent s.d. (* $P < 0.05$; *** $P < 0.001$). (C) Quantification of PH3+ cells/body area after 1 week of *bls2/3/5* RNAi treatment (n of controls=5, n of RNAi=9, * $P < 0.05$), and the corresponding anti-PH3 immunostaining images showing the increment of the mitotic cells. (D) Anti-PH3 immunostaining images of *bls2/3/5* RNAi animals and controls showing the increment of the mitotic cells after 3 weeks of the treatment. (E) TUNEL assay images of *bls2/3/5*

RNAi animals and controls, corresponding to transversal sections of the animals. TUNEL+ cells/section area was quantified. At least 9 sections per animal and at least 5 animals per condition were analyzed (F) Quantification of nuclei of epidermal cells stained with DAPI per area (n of controls=15, n of RNAi=15, *** $P<0.001$). The illustration indicates the area quantified with a black square. (G) Confocal images of the expression of neural (*th*) and chemoreceptor (*cintillo*) markers in *bls2/3/5* RNAi animals and controls. The illustration shows the expression of *th* and *cintillo*, and the square indicates the area analyzed. Images from C and F correspond to Z projections. Scale bars: 200 μm in the entire panel.

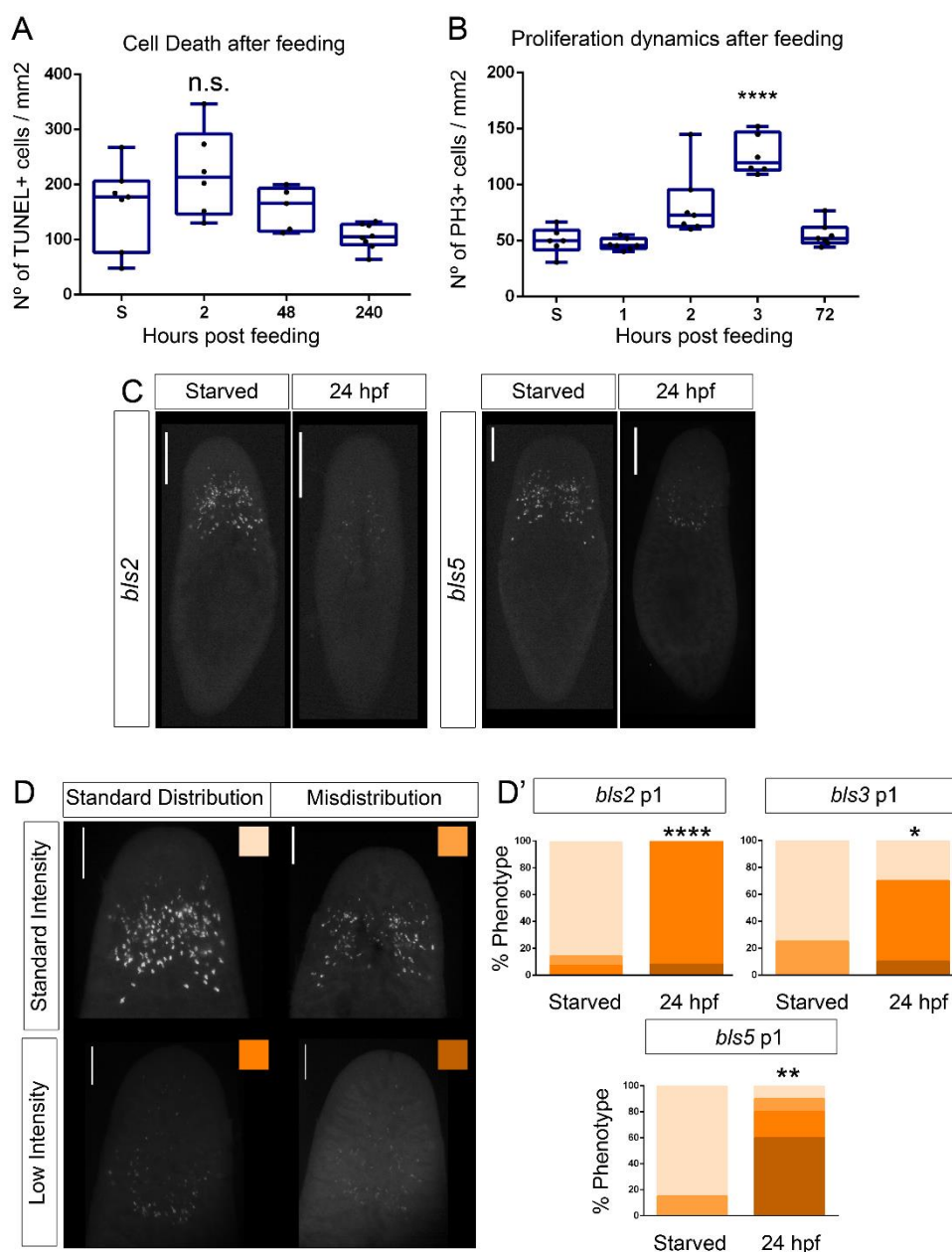


Figure S7. *bls2*, *bls3* and *bls5* are down-regulated by food ingestion. (A) TUNEL assay at different time points after feeding reveals no changes in wild type planarians (n of starved=7, n of 2hpf=6, n.s.). (B) PH3+ cells/body area quantification at different time points after feeding reveals a proliferative peak at 3hpf (n of starved=6, n of 3hpf=6, **** $P < 0.0001$). (C) Representative FISH images of *bls2* and *bls5* before feeding and after feeding, demonstrating its reduced expression at 24 hpf. (D) Representative FISH images showing the downregulation and delocalization of *bls2*, *bls3*, and *bls5* expression observed after feeding. Four patterns of *bls2*, *bls3*, and *bls5* expression could be observed: high intensity and localized; high intensity and

delocalized; low intensity and localized; low intensity and delocalized. (The brightness and contrast of the images is not equivalent, since in the low density ones it had to be adjusted to show the expression). The percentages corresponding to each category are shown in Dq (starvation conditions, $n > 7$; 24 hpf, $n > 10$; * $P < 0.05$, ** $P < 0.01$, **** $P < 0.0001$).